Available online at www.sciencedirect.com
SCIENCE DIRECT®
Annals of Physics 321 (2006) 1025–1062
ANNALS of PHYSICS
www.elsevier.com/locate/aop

Wavepacket dynamics, quantum reversibility, and random matrix theory

Moritz Hiller [a,*], Doron Cohen [b], Theo Geisel [a], Tsampikos Kottos [a,c]

[a] *Max Planck Institute for Dynamics and Self-Organization and Department of Physics, University of Göttingen, Bunsenstraße 10, D-37073 Göttingen, Germany*
[b] *Department of Physics, Ben-Gurion University, Beer-Sheva 84105, Israel*
[c] *Department of Physics, Wesleyan University, Middletown, CT 06459, USA*

Received 14 June 2005; accepted 7 December 2005
Available online 9 February 2006

Abstract

We introduce and analyze the physics of "driving reversal" experiments. These are prototype wavepacket dynamics scenarios probing quantum irreversibility. Unlike the mostly hypothetical "time reversal" concept, a "driving reversal" scenario can be realized in a laboratory experiment, and is relevant to the theory of quantum dissipation. We study both the energy spreading and the survival probability in such experiments. We also introduce and study the "compensation time" (time of maximum return) in such a scenario. Extensive effort is devoted to figuring out the capability of either linear response theory or random matrix theory (RMT) to describe specific features of the time evolution. We explain that RMT modeling leads to a strong non-perturbative response effect that differs from the semiclassical behavior.

PACS: 03.65.−w; 03.65.Sq; 05.45.Mt; 73.23.−b

Keywords: Quantum dissipation; Quantum chaos; Random matrix theory

* Corresponding author.
E-mail address: mhiller@chaos.gwdg.de (M. Hiller).

0003-4916/$ - see front matter
doi:10.1016/j.aop.2005.12.003

1. Introduction

In recent years there has been an increasing interest in understanding the theory of driven quantized chaotic systems [1–11]. Driven systems are described by a Hamiltonian $\mathcal{H}(Q,P,x(t))$, where $x(t)$ is a time-dependent parameter and (Q,P) are some generalized actions. Due to the time dependence of $x(t)$, the energy of the system is not a constant of motion. Rather the system makes "transitions" between energy levels, and therefore absorbs energy. This irreversible loss of energy is known as *dissipation*. To have a clear understanding of quantum dissipation we need a theory for the time evolution of the energy distribution.

Unfortunately, our understanding on quantum dynamics of chaotic systems is still quite limited. The majority of the existing quantum chaos literature concentrates on understanding the properties of eigenfunctions and eigenvalues. One of the main outcomes of these studies is the conjecture that random matrix theory (RMT) modeling, initiated half a century ago by Wigner [12,13], can capture the *universal* aspects of quantum chaotic systems [14,15]. Due to its large success RMT has become a major theoretical tool in quantum chaos studies [14,15], and it has found applications in both nuclear and mesoscopic physics (for a recent review see [16]). However, its applicability to quantum dynamics was left unexplored [17,18].

This paper extends our previous reports [10,17,18] on quantum *dynamics*, both in detail and depth. Specifically, we analyze two dynamical schemes: the first is the so-called wave-packet dynamics associated with a rectangular pulse of strength $+\epsilon$ which is turned on for a specified duration. The second involves an additional pulse followed by the first one which has a strength $-\epsilon$ and is of equal duration. We define this latter scheme as *driving reversal* scenario. We illuminate the direct relevance of our study with the studies of quantum irreversibility of energy spreading [10] and consequently with quantum dissipation. We investigate the conditions under which maximum compensation is succeeded and define the notion of compensation (echo) time. To this end we rely both on numerical calculations performed for a chaotic system and on analytical considerations based on linear response theory (LRT). The latter constitutes the leading theoretical framework for the analysis of driven systems and our study aims to clarify the limitations of LRT due to chaos. Our results are always compared with the outcomes of RMT modeling. We find that the RMT approach fails in general, to give the correct picture of wave-evolution. RMT can be trusted only to the extend that it gives trivial results that are implied by perturbation theory. Non-perturbative effects are sensitive to the underlying classical dynamics, and therefore the $\hbar \to 0$ behavior for effective RMT models is strikingly different from the correct semiclassical limit.

The structure of this paper is as follows: in the next section, we discuss the notion of irreversibility which is related to driving reversal schemes and distinguish it from micro-reversibility which is associated with time reversal experiments. In Section 3 we discuss the driving schemes that we are using and we introduce the various observables that we will study in the rest of the paper. In Section 4, the model systems are introduced and an analysis of the statistical properties of the eigenvalues and the Hamiltonian matrix is presented. The random matrix theory modeling is presented in Subsection 4.4. In Section 5 we introduce the concept of parametric regimes and exhibit its applicability in the analysis of parametric evolution of eigenstates [19]. Section 6 extends the notion of regimes in dynamics and presents the results of linear response theory for the variance and the

survival probability. The linear response theory (LRT) for the variance is analyzed in details in the following Subsection 6.1. In this subsection, we also introduce the notion of restricted quantum-classical correspondence (QCC) and show that, as far as the second moment of the evolving wavepacket is concerned, both classical and quantum mechanical LRT coincide. In Section 6.5 we present in detail the results of LRT for the survival probability for the two driving schemes that we analyze. The following Sections 7 and 8 contain the results of our numerical analysis together with a critical comparison with the theoretical predictions obtained via LRT. Specifically in Section 7, we present an analysis of wavepacket dynamics [18] and expose the weakness of RMT strategy to describe wavepacket dynamics. In Section 8 we study the evolution in the second half of the driving period and analyze the Quantum Irreversibility in energy spreading, where strong non-perturbative features are found for RMT models [10]. Section 9 summarizes our findings.

2. Reversibility

The dynamics of either a classical or a quantum mechanical system is generated by a Hamiltonian $\mathcal{H}(Q,P;x(t))$, where $x=(X_1,X_2,X_3,\ldots)$ is a set of parameters that can be controlled from the "outside." In principle, x stands for the infinite set of parameters that describe the electric and magnetic fields acting on the system. But in practice the experimentalist can control only few parameters. A prototype example is a gas of particles inside a container with a piston. Then X_1 may be the position of the piston, X_2 may be some imposed electric field, and X_3 may be some imposed magnetic field. Another example is electrons in a quantum dot where some of the parameters X represent gate voltages.

What do we mean by reversibility? Let us assume that the system evolves for some time. The evolution is described by

$$U[x]=\exp\left(-\frac{\mathrm{i}}{\hbar}\int_0^t \mathcal{H}(x(t'))\mathrm{d}t'\right), \tag{1}$$

where Exp stands for time ordered exponentiation. In the case of the archetype example of a container with gas particles, we assume that there is a piston (position X) that is translated outwards ($X^A(t)$ increasing). Then we would "undo" the evolution, by displacing the piston "inwards" ($X^B(t)$ decreasing). In such a case the complete evolution is described by $U[x]=U[x^B]U[x^A]$. If we get $U=1$ (up to a phase factor), then it means that it is possible to bring the system back to its original state. In this case, we say that the process $U[x]$ is reversible.

In the strict adiabatic limit the above described process is indeed reversible. What about the non-adiabatic case? To have a well posed question we would like to distinguish below between "time reversal" and "driving reversal" schemes.

2.1. Time reversal scheme

Obviously, we are allowed to invent very complicated schemes to "undo" the evolution. The ultimate scheme (in the case of the above example) involves reversal of the velocities. Assume that this operation is represented by U_T, then the reverse evolution is described by

$$U_{\text{reverse}}=U_T U[x^B]U_T, \tag{2}$$

where in $x_B(t)$ we have the time reversed piston displacement ($X(t)$) together with the sign of the magnetic field (if it exists) should be inverted. The question is whether U_T can be realized. If we postulate that any unitary or anti-unitary transformation can be realized, then it follows trivially that any unitary evolution is "micro-reversible." But when we talk about reversibility (rather than micro-reversibility) we allow control over a restricted set of parameters (fields). Then the question is whether we can find a driving scheme, named x^T, such that

$$U_T = U[x^T] \quad ??? \tag{3}$$

With such restriction it is clear that in general the evolution is not reversible.

Recently, it has been demonstrated in an actual experiment that the evolution of a spin system (cluster with many interacting spins) can be reversed. Namely, the complete evolution was described by $U[x] = U[x^T]U[x^A]U[x^T]U[x^A]$, where $U[x^A]$ is generated by some Hamiltonian $\mathcal{H}_A = \mathcal{H}_0 + \varepsilon\mathcal{W}$. The term $\mathcal{H}_0$ represents the interaction between the spins, while the term $\mathcal{W}$ represents some extra interactions. The unitary operation $U[x^T]$ is realized using NMR techniques, and its effect is to invert the signs of all the couplings. Namely, $U[x^T]\mathcal{H}_0U[x^T] = -\mathcal{H}_0$. Hence, the reversed evolution is described by

$$U_{\text{reverse}} = \exp\left(-\frac{\mathrm{i}}{\hbar}t(-\mathcal{H}_0 + \varepsilon\mathcal{W})\right), \tag{4}$$

which is the so-called Loschmidt Echo scenario. In principle, we would like to have $\varepsilon = 0$ so as to get $U = 1$, but in practice we have some un-controlled residual fields that influence the system, and therefore $\varepsilon \neq 0$. There is a huge amount of literature that discusses what happens in such scenario [20–24].

2.2. Driving reversal scheme

The above described experiment is in fact exceptional. In most cases it is possible to invert the sign of only one part of the Hamiltonian, which is associated with the driving field. Namely, if for instance $U[x^A]$ is generated by $\mathcal{H}_A = H_0 + \varepsilon\mathcal{W}$, then we can realize

$$U_{\text{reverse}} = \exp\left(-\frac{\mathrm{i}}{\hbar}t(\mathcal{H}_0 - \varepsilon\mathcal{W})\right), \tag{5}$$

whereas Eq. (4) cannot be realized in general. We call such a typical scenario "driving reversal" to distinguish it from "time reversal" (Loschmidt Echo) scenario.

The study of "driving reversal" is quite different from the study of "Loschmidt Echo." A simple minded point of view is that the two problems are formally equivalent because we simply permute the roles of $\mathcal{H}_0$ and $\mathcal{W}$. In fact, there is no symmetry here. The main part of the Hamiltonian has in general an unbounded spectrum with well defined density of states, while the perturbation $\mathcal{W}$ is assumed to be bounded. This difference completely changes the "physics" of dynamics.

To conclude the above discussion we would like to emphasize that micro-reversibility is related to "time reversal" experiments which in general cannot be realized, while the issue of reversibility is related to "driving reversal," which in principle can be realized. Our distinction reflects the simple observation that not any unitary or anti-unitary operation can be realized.

3. Object of the study

In this paper, we consider the issue of irreversibility for quantized chaotic systems. We assume for simplicity one parameter driving. We further assume that the variation of $x(t)$ is small in the corresponding classical system so that the analysis can be carried out with a linearized Hamiltonian. Namely,

$$\mathcal{H}(Q,P;x(t)) \approx \mathcal{H}_0 + \delta x(t)\mathcal{W}, \tag{6}$$

where $\mathcal{H}_0 \equiv \mathcal{H}(Q,P;x(0))$ and $\delta x = x(t) - x(0)$. For latter purposes it is convenient to write the perturbation as

$$\delta x(t) = \varepsilon \times f(t), \tag{7}$$

where ε controls the "strength of the perturbation," while $f(t)$ is the scaled time dependence. Note that if $f(t)$ is a step function, then ε is the "size" of the perturbation, while if $f(t) \propto t$ then ε is the "rate" of the driving. In the representation of $\mathcal{H}_0$ we can write

$$\mathcal{H} = \boldsymbol{E} + \delta x(t)\boldsymbol{B}, \tag{8}$$

where by convention the diagonal terms of $\boldsymbol{B}$ are absorbed into the diagonal matrix $\boldsymbol{E}$. From general considerations that we explain later it follows that $\boldsymbol{B}$ is a banded matrix that looks random. This motivates the study of an effective banded random matrix (EBRM) model, as well as its simplified version which is the standard Wigner banded random matrix (WBRM) model (see detailed definitions in the following).

To study the irreversibility for a given driving scenario, we have to introduce measures that quantify the departure from the initial state. We define a set of such measures in the following subsections.

3.1. The evolving distribution $P_t(n|n_0)$

Given the Hamiltonian $\mathcal{H}(Q,P;x)$, an initial preparation at state $|n_0\rangle$, and a driving scenario $x(t)$, it is most natural to analyze the evolution of the probability distribution

$$P_t(n|n_0) = |\langle n|U(t)|n_0\rangle|^2. \tag{9}$$

We always assume that $x(t) = x(0)$.

By convention we order the states by their energy. Hence, we can regard $\mathcal{P}_t(n|n_0)$ as a function of $r = n - n_0$, and average over the initial preparation, so as to get a smooth distribution $\mathcal{P}_t(r)$.

The survival probability is defined as

$$\mathcal{P}(t) = |\langle n_0|U(t)|n_0\rangle|^2 = P_t(n_0|n_0), \tag{10}$$

and the energy spreading is defined as

$$\delta E(t) = \sqrt{\sum_n P_t(n|n_0)(E_n - E_{n_0})^2}. \tag{11}$$

These are the major measures for the characterization of the distribution. In later sections we would like to analyze their time evolution.

The physics of $\delta E(t)$ is very different from the physics of $\mathcal{P}(t)$ because the former is very sensitive to the tails of the distribution. Yet, the actual "width" of the distribution is not

captured by any of these measures. A proper measure for the width can be defined as follows:

$$\delta E_{\mathrm{core}}(t) = [n_{75\%} - n_{25\%}]\Delta, \tag{12}$$

where Δ is the mean level spacing and n_q is determined through the equation $\sum_n P_t(n|n_0) = q$. Namely, it is the width of the main body of the distribution. Still another characteristic of the distribution is the participation ratio $\delta n_{\mathrm{IPR}}(t)$. It gives the number of levels that are occupied at time t by the distribution. The ratio $\delta n_{\mathrm{IPR}}/(n_{75\%} - n_{25\%})$ can be used as a measure for sparsity. We assume in this paper strongly chaotic systems, so sparsity is not an issue and $\delta n_{\mathrm{IPR}} \sim \delta E_{\mathrm{core}}/\Delta$.

3.2. The compensation time t_r

In this paper, we consider two types of driving schemes. Both driving schemes are presented schematically in Fig. 1.

The first type of scheme is the *wavepacket dynamics* scenario for which the driving is turned-on at time $t = 0$ and turned-off at a later time $t = T$.

The second type of scenario that we investigate is what we call *driving reversal*. In this scenario the initial rectangular pulse is followed by a compensating pulse of equal duration. The total period of the cycle is T.

In Fig. 9 we show representative results for the time evolution of $\delta E(t)$ in a wavepacket scenario, while in Fig. 12 we show what happens in case of a driving reversal scenario. Corresponding plots for $\mathcal{P}(t)$ are presented in Fig. 13. We shall define the models and we shall discuss the details of these figures later on. At this stage, we would like to motivate by inspection of these figures the definition of "compensation time."

We define the compensation time t_r, as the time after the driving reversal, when maximum compensation (maximum return) is observed. If it is determined by the maximum of the survival probability kernel $\mathcal{P}(t)$, then we denote it as t_r^P. If it is determined by the minimum of the energy spreading $\delta E(t)$ then we denote it as t_r^E. It should be remembered that the theory of $\mathcal{P}(t)$ and $\delta E(t)$ is not the same, hence the distinction in the notation. The time of maximum compensation is in general not $t_r = T$ but rather

$$T/2 < t_r < T. \tag{13}$$

We emphasize this point because the notion of "echo," as used in the literature, seems to reflect a false assertion [24].

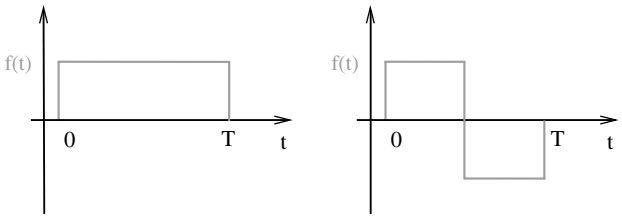

Fig. 1. Shape of the applied driving schemes $f(t)$; wavepacket dynamics (left panel) and driving reversal scenario (right panel).

For the convenience of the reader we concentrate in the following table on the major notations in this paper:

Notation	Explanation	Reference
$\mathcal{H}(Q,P;x(t))$	Classical linearized Hamiltonian	Eq. (6)
$\mathcal{F}(t)$	Generalized force	Eq. (17)
$C(\tau)$	Correlation function	Eq. (18)
τ_{cl}	Correlation time	—
$\tilde{C}(\omega)$	Fluctuation spectrum	Eq. (19)
$\mathcal{H} = \boldsymbol{E} + \delta x \boldsymbol{B}$	The Hamiltonian matrix	Eq. (8)
2DW	The physical model system	Eq. (14)
EBRM	The corresponding RMT model	—
WBRM	The Wigner RMT model	—
Δ	Mean level spacing	Eq. (23)
Δ_b	Energy bandwidth	Eq. (24)
σ	RMS of near diagonal couplings	—
$P_{\mathrm{spacings}}(s)$	Energy spacing distribution	Eq. (16)
$P_{\mathrm{couplings}}(q)$	Distribution of couplings	Eq. (25)
$E_n(x)$	Eigenenergies of the Hamiltonian	—
$E_n - E_m \approx r\Delta$	Estimated energy difference for $r = n - m$	—
$P(n\|m)$	Overlaps of eigenstates given a constant perturbation ε	Eq. (27)
$P(r)$	Smoothed version of $P(n\|m)$	—
$\Gamma(\delta x)$	The number of levels that are mixed non-perturbatively	—
$\delta E_{\mathrm{cl}} \propto \delta x$	The classical width of the LDoS	Eq. (29)
$\delta x = \varepsilon f(t)$	Driving scheme	Eq. (7)
T	The period of the driving cycle (if applicable)	—
$P_t(n\|m)$	The transition probability	Eq. (9)
$P_t(r)$	Smoothed version of $P_t(n\|n_0)$	—
$\mathcal{P}(t)$	The survival probability $P_t(n_0\|n_0)$	Eq. (10)
$p(t) = 1 - \mathcal{P}(t)$	Total transition probability	Eq. (47)
$\delta E(t)$	Energy spreading	Eq. (11)
$\delta E_{\mathrm{core}}(t)$	The "core" width of the distribution	Eq. (12)
t_r^P	Compensation time for the survival probability	—
t_r^E	Compensation time for the energy spreading	—
t_{prt}, t_{sdn}, t_{erg}	Various time scales in the dynamics	Eqs. (59), (62), (70)
ε_c, $\varepsilon_{\mathrm{prt}}$	Borders between regimes	Eqs. (31), (33)
$P_{\mathrm{FOPT}}, P_{\mathrm{prt}}, P_{\mathrm{sc}}$	Various approximations to $P()$	Eqs. (30), (32), (34), (35)

4. Modeling

We are interested in quantized chaotic systems that have few degrees of freedom. The dynamical system used in our studies is the Pullen–Edmonds model [25,26]. It consists of two harmonic oscillators that are non-linearly coupled. The corresponding Hamiltonian is

$$\mathcal{H}(Q,P;x) = \tfrac{1}{2}(P_1^2 + P_2^2 + Q_1^2 + Q_2^2) + xQ_1^2Q_2^2. \tag{14}$$

The mass and the frequency of the harmonic oscillators are set to one. Without loss of generality we set $x(0) = x_0 = 1$. Later, we shall consider classically small deformations ($\delta x \ll 1$) of the potential. One can regard this model (14) as a description of a particle moving in a two dimensional well (2DW). The energy E is the only dimensionless parameter of the classical motion. For high energies $E > 5$ the motion of the Pullen–Edmonds model is ergodic. Specifically, it was found that the measure of the chaotic component on the Poincaré section deviates from unity by no more than 10^{-3} [25,26].

In Fig. 2, we display the equipotential contours of the model Hamiltonian (14) with $x_0 = 1$. We observe that the equipotential surfaces are circles but as the energy is increased they become more and more deformed leading to chaotic motion. Our analysis is focused on an energy window around $E \sim 3$ where the motion is mainly chaotic. This is illustrated in the right panel of Fig. 2 where we report the Poincaré section (of the phase space) of a selected trajectory, obtained from $\mathcal{H}_0$ at $E = 3$. The ergodicity of the motion is illustrated by the Poincaré section, filling the plane except from some tiny quasi-integrable islands.

The perturbation is described by $\mathcal{W} = Q_1^2Q_2^2$. In the classical analysis there is only one significant regime for the strength of the perturbation. Namely, the perturbation is considered to be classically small if

$$\delta x \ll \varepsilon_{\rm cl}, \tag{15}$$

where $\varepsilon_{\rm cl} = 1$. This is the regime where (classical) linear analysis applies. Namely, within this regime the deformation of the energy surface $\mathcal{H}_0 = E$ can be described as a linear process [see Eq. (29)].

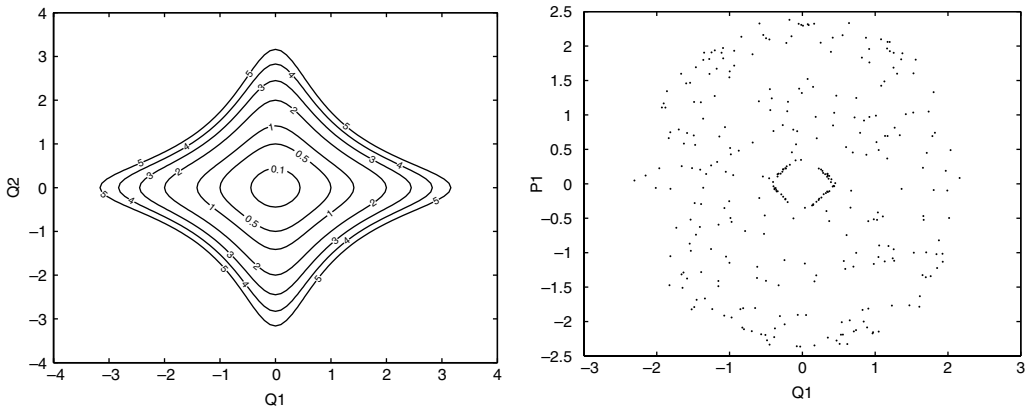

Fig. 2. Equipotential contours (left) of the model Hamiltonian $\mathcal{H}_0$ for different energies and the Poincaré section (right) of a selected trajectory at $E = 3$. Some tiny quasi-integrable islands are avoided (mainly at $(0,0)$).

4.1. Energy levels

Let us now quantize the system. For obvious reasons we are considering a de-symmetrized 1/8 well with Dirichlet boundary conditions on the lines $Q_1 = 0$, $Q_2 = 0$ and $Q_1 = Q_2$. The matrix representation of $\mathcal{H}_0$ in the basis of the un-coupled system is very simple. The eigenstates of the Hamiltonian $\mathcal{H}_0$ are then obtained numerically.

As mentioned above, we consider the experiments to take place in an energy window $2.8 < E < 3.1$ which is classically small and where the motion is predominantly chaotic. Nevertheless, quantum mechanically, this energy window is large, i.e., many levels are found therein. The local mean level spacing $\Delta(E)$ at this energy range is given approximately by $\Delta \sim 4.3\hbar^2$. The smallest $\hbar$ that we can handle is $\hbar = 0.012$ resulting in a matrix size of about 4000×4000. Unless stated otherwise, all the numerical data presented below correspond to a quantization with $\hbar = 0.012$.

As it was previously mentioned in the introduction, the main focus of quantum chaos studies has so far been on issues of spectral statistics [14,15]. In this context it turns out that the sub$-\hbar$ statistical features of the energy spectrum are "universal," and obey the predictions of RMT. In particular, we expect that the level spacing distribution $P(s)$ of the "unfolded" (with respect to Δ) level spacings $s_n = (E_{n+1} - E_n)/\Delta$ will follow with high accuracy the so-called *Wigner surmise*. For systems with time reversal symmetry it takes the form [14,27]

$$P_{\text{spacings}}(s) = \frac{\pi}{2} s e^{-\frac{\pi}{4}s^2} \tag{16}$$

indicating that there is a linear repulsion between nearby levels. Non-universal (i.e., system specific) features are reflected only in the large scale properties of the spectrum and constitute the fingerprints of the underlying classical chaotic dynamics.

The de-symmetrized 2DW model shows time reversal symmetry, and therefore we expect the distribution to follow Eq. (16). The analysis is carried out only for the levels contained in the chosen energy window around $E = 3$. Instead of plotting $P(s)$ we show the integrated distribution $I(s) = \int_0^s P(s')\mathrm{d}s'$, which is independent of the bin size of the histogram. In Fig. 3 we present our numerical data for $I(s)$ while the inset shows the deviations from the theoretical prediction (16). The agreement with the theory is fairly good and the level repulsion is clearly observed. The observed deviations have to be related on the one hand to the tiny quasi-integrable islands that exist at $E = 3$ as well as to rather limited level statistics.

4.2. The band-profile

In this subsection, we explain that the band-structure of $\boldsymbol{B}$ is related to the fluctuations of the classical motion. This is the major step towards RMT modeling.

Consider a given ergodic trajectory $(Q(t), P(t))$ on the energy surface $\mathcal{H}(Q(0), P(0); x_0) = E$. An example is shown in the right panel of Fig. 2. We can associate with it a stochastic-like variable

$$\mathcal{F}(t) = -\frac{\partial \mathcal{H}}{\partial x}(Q(t), P(t), x(t)), \tag{17}$$

which for our linearized Hamiltonian is simply the perturbation term $\mathcal{F} = -\mathcal{W} = -Q_1^2 Q_2^2$. It can be interpreted as the generalized force that acts on the boundary of the 2D well. It

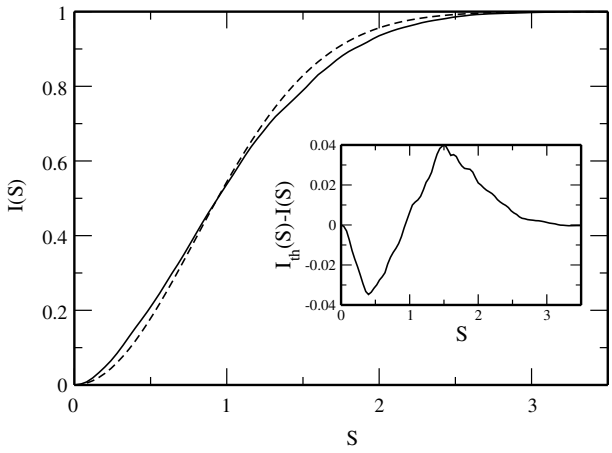

Fig. 3. The integrated level spacing distribution $I(S)$ of the unperturbed Hamiltonian $\mathcal{H}_0$ ($\hbar = 0.012$). The dashed line is the theoretical prediction for the GOE. Inset: difference between the theoretical prediction $I_{\rm th}(S)$ and the actual distribution $I(S)$.

may have a non-zero average ("conservative" part) but below we are interested only in its fluctuations.

To characterize the fluctuations of $\mathcal{F}(t)$ we introduce the autocorrelation function $C(\tau)$

$$C(\tau) = \langle \mathcal{F}(t)\mathcal{F}(t+\tau)\rangle - \langle \mathcal{F}^2\rangle. \tag{18}$$

The angular brackets denote an averaging which is either micro-canonical over some initial conditions $(Q(0), P(0))$ or temporal (due to the assumed ergodicity). The power spectrum for the 2D well model is shown in Fig. 4 (see solid line).

For generic chaotic systems (described by smooth Hamiltonians), the fluctuations are characterized by a short correlation time $\tau_{\rm cl}$, after which the correlations are negligible. In generic circumstances $\tau_{\rm cl}$ is essentially the ergodic time. For our model system $\tau_{\rm cl} \sim 1$.

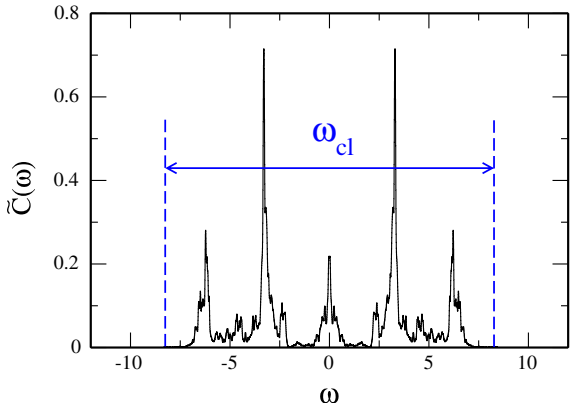

Fig. 4. The classical power-spectrum of the model (14). The classical cut-off frequency $\omega_{\rm cl} \simeq 7$ is indicated by perpendicular dashed lines.

The power spectrum of the fluctuations $\tilde{C}(\omega)$ is defined by a Fourier transform:

$$\tilde{C}(\omega) = \int_{-\infty}^{\infty} C(\tau) \exp(\mathrm{i}\omega\tau)\mathrm{d}\tau. \tag{19}$$

This power spectrum is characterized by a cut-off frequency ω_{cl} which is inversely proportional to the classical correlation time

$$\omega_{\mathrm{cl}} = \frac{2\pi}{\tau_{\mathrm{cl}}}. \tag{20}$$

Indeed in the case of our model system we get $\omega_{\mathrm{cl}} \sim 7$ which is in agreement with Fig. 4.

The implication of having a short but non-vanishing classical correlation time τ_{cl} is having large but finite bandwidth in the perturbation matrix $\boldsymbol{B}$. This follows from the identity

$$\tilde{C}(\omega) = \sum_n |\boldsymbol{B}_{nm}|^2 2\pi\delta\left(\omega - \frac{E_n - E_m}{\hbar}\right), \tag{21}$$

which implies [28]

$$\langle |\boldsymbol{B}_{nm}|^2 \rangle = \frac{\Delta}{2\pi\hbar}\tilde{C}\left(\omega = \frac{E_n - E_m}{\hbar}\right). \tag{22}$$

Hence, the matrix elements of the perturbation matrix $\boldsymbol{B}$ are extremely small outside of a band of width $b = \hbar\omega_{\mathrm{cl}}/\Delta$.

In the inset of Fig. 5, we show a snapshot of the perturbation matrix $|\boldsymbol{B}_{nm}|^2$. It clearly shows a band-structure. At the same figure, we also display the band-profiles for different values of $\hbar$. A good agreement with the classical power spectrum $\tilde{C}(\omega)$ is evident.

It is important to realize that upon quantization we end up with *two* distinct energy scales. One is obviously the mean level spacing (see previous subsection)

$$\Delta \propto \hbar^d, \tag{23}$$

where the dimensionality is $d = 2$ in case of our model system. The other energy scale is the bandwidth

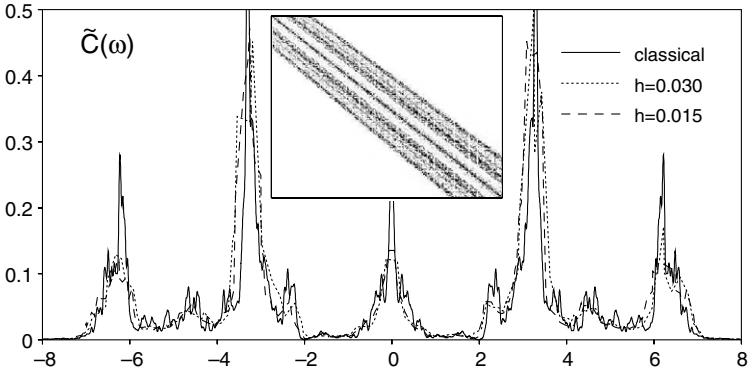

Fig. 5. The band-profile $(2\pi\hbar/\Delta)\cdot|\boldsymbol{B}_{nm}|^2$ versus $\omega = (E_n - E_m)/\hbar$ is compared with the classical power spectrum $\tilde{C}(\omega)$. Inset: a snapshot of the perturbation matrix $\boldsymbol{B}$.

$$\Delta_b = \frac{2\pi\hbar}{\tau_{\rm cl}} = b\Delta. \tag{24}$$

This energy scale is also known in the corresponding literature as the "non-universal" energy scale [29], or (in case of diffusive motion) as the Thouless energy [30].[1] One has to notice that deep in the semiclassical limit $\hbar \to 0$ these two energy scales differ enormously from one another (provided $d \geqslant 2$). We shall see in the following sections that this scale separation has dramatic consequences in the theory of driven quantum systems.

4.3. Distribution of couplings

We investigate further the statistical properties of the matrix elements $\boldsymbol{B}_{nm}$ of the perturbation matrix, by studying their distribution. RMT assumes that upon appropriate unfolding they must be distributed in a Gaussian manner. The 'unfolding' aims to remove system specific properties and reveal the underlying universality. It is done by normalizing the matrix elements with the local standard deviation $\sigma = \sqrt{\langle |\boldsymbol{B}_{nm}|^2 \rangle}$ related through Eq. (22) with the classical power spectrum $\tilde{C}(\omega)$.

The existing literature is not conclusive about the distribution of the normalized matrix elements $q = \boldsymbol{B}_{nm}/\sigma$. Specifically, Berry [31] and more recently Prosen [32,33], claimed that $\mathcal{P}(q)$ should be Gaussian. On the other hand, Austin and Wilkinson [34] have found that the Gaussian is approached only in the limit of high quantum numbers while for small numbers, i.e., low energies, a different distribution applies, namely

$$P_{\rm couplings}(q) = \frac{\Gamma\left(\frac{N}{2}\right)}{\sqrt{\pi N}\,\Gamma\left(\frac{N-1}{2}\right)} \left(1 - \frac{q^2}{N}\right)^{(N-3)/2}. \tag{25}$$

This is the distribution of the elements of an N-dimensional vector, distributed randomly over the surface of an N-dimensional sphere of radius $\sqrt{N}$. For $N \to \infty$ this distribution approaches a Gaussian.

The distribution $\mathcal{P}(q)$ for our model is reported in Fig. 6. The solid line corresponds to a Gaussian of unit variance while the dashed-dotted line is obtained by fitting Eq. (25) to the numerical data using N as a fitting parameter. We observe that the Gaussian resembles better our numerical data although deviations, especially for matrix elements close to zero, can be clearly seen. We attribute these deviations to the existence of the tiny stability islands in the phase space. Trajectories started in those islands cannot reach the chaotic sea and vice versa. Quantum mechanically the consequence of this would be vanishing matrix elements $\boldsymbol{B}_{nm}$ which represent the classically forbidden transitions.

4.4. RMT modeling

It was the idea of Wigner [12,13] more than 40 years ago, to study a simplified model, where the Hamiltonian is given by Eq. (8), and where $\boldsymbol{B}$ is a Banded *Random* Matrix (BRM) [35–37]. The diagonal matrix $\boldsymbol{E}$ has elements which are the ordered energies $\{E_n\}$, with mean level spacing Δ. The perturbation matrix $\boldsymbol{B}$ has a *rectangular* band-profile

[1] The dimensionless parameter b scales like $b \propto \hbar^{-(d-1)}$ and in the frame of mesoscopic systems is recognized as the dimensionless Thouless conductance [30].

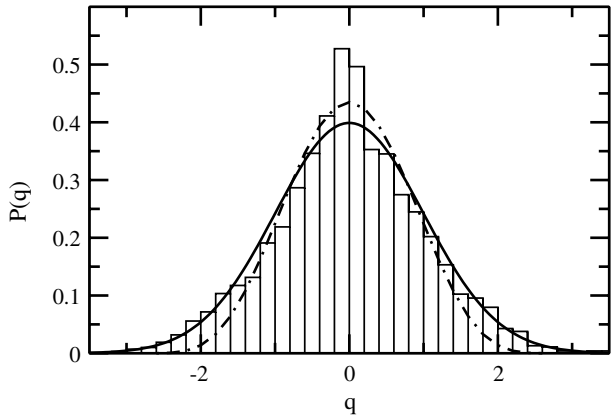

Fig. 6. Distribution of matrix elements q around $E = 3$ rescaled with the averaged band-profile. The solid black line corresponds to a Gaussian distribution with unit variance while the dashed-dotted line corresponds to a fit from Eq. (25) with a fitting parameter $N = 7.8$. The quantization corresponds to $\hbar = 0.03$.

of band-size b. Within the band $0 < |n - m| \leqslant b$ the elements are independent random variables given by a Gaussian distribution with zero mean and a variance $\sigma^2 = \langle |\boldsymbol{B}_{nm}|^2 \rangle$. Outside the band they vanish. We refer to this model as the *Wigner BRM* model (WBRM).

Given the band-profile, we can use Eq. (22) in reverse direction to calculate the correlation function $C(\tau)$. For the WBRM model we get

$$C(\tau) = 2\sigma^2 b \mathrm{sinc}(\tau/\tau_{\mathrm{cl}}), \tag{26}$$

where $\tau_{\mathrm{cl}} = \hbar/\Delta_b$. Thus, there are three parameters (Δ, b, σ) that define the WBRM model.

The WBRM model can be regarded as a *simplified* local description of a true Hamiltonian matrix. This approach is attractive both analytically and numerically. Analytical calculations are greatly simplified by the assumption that the off-diagonal terms can be treated as independent random numbers. Also from a numerical point of view it is quite a tough task to calculate the true matrix elements of the $\boldsymbol{B}$ matrix. It requires a preliminary step where the chaotic $\mathcal{H}_0$ is diagonalized. Due to memory limitations one ends up with quite small matrices. For the Pullen–Edmonds model we were able to handle matrices of final size $N = 4000$ maximum. This should be contrasted with the WBRM simulations, where using self-expanding algorithm [17,41] we were able to handle system sizes up to $N = 100{,}000$ along with significantly reduced CPU time.

We would like to stress again that the underlying assumption of WBRM, namely that the off-diagonal elements are *uncorrelated* random numbers, has to be treated with extreme care.

The WBRM model involves an additional simplification. Namely, one assumes that $\boldsymbol{B}$ has a *rectangular* band-profile. A simple inspection of the band-profile of our model Eq. (14) shows that this is not the case (see Fig. 5). We eliminate this simplification by introducing a RMT model that is even closer to the dynamical one. To this end, we randomize the signs of the off-diagonal elements of the perturbation matrix $\boldsymbol{B}$ keeping its band-structure intact. This procedure leads to a random model that exhibits only universal properties while it lacks any semiclassical limit. We will refer to it as the *effective* banded random matrix model (EBRM).

5. The parametric evolution of the eigenfunctions

As we change the parameter δx in the Hamiltonian Eq. (8), the instantaneous eigenstates $\{|n(x)\rangle\}$ evolve and undergo structural changes. To understand the actual dynamics, it is important to understand these structural changes. This leads to the introduction of

$$P(n|m) = |\langle n(x)|m(x_0)\rangle|^2, \tag{27}$$

which is easier to analyze than $P_t(n|n_0)$. Up to some trivial scaling and shifting $P(n|m)$ is essentially the local density of states (LDoS):

$$P(E|m) = \sum_n |\langle n(x)|m(x_0)\rangle|^2 \delta(E - E_n). \tag{28}$$

The averaged distribution $P(r)$ is defined in complete analogy with the definition of $P_t(r)$. Namely, we use the notation $r = n - m$, and average over several m states with roughly the same energy $E_m \sim E$.

Generically $P(r)$ undergoes the following structural changes as a function of growing δx. We first summarize the generic picture, which involves the parametric scales ε_c and $\varepsilon_{\rm prt}$. and the approximations $P_{\rm FOPT}$, $P_{\rm prt}$, and $P_{\rm sc}$. Then we discuss how to determine these scales, and what these approximations are.

- The first order perturbative theory (FOPT) regime is defined as the range $\delta x < \varepsilon_c$ where we can use FOPT to get an approximation that we denote as $P() \approx P_{\rm FOPT}$.
- The (extended) perturbative regime is defined as the range $\varepsilon_c < \delta x < \varepsilon_{\rm prt}$ where we can use perturbation theory (to infinite order) to get a meaningful approximation that we denote as $P() \approx P_{\rm prt}$. Obviously, $P_{\rm prt}$ reduces to $P_{\rm FOPT}$ in the FOPT regime.
- The non-perturbative regime is defined as the range $\delta x > \varepsilon_{\rm prt}$ where perturbation theory becomes non-applicable. In this regime, we have to use either RMT or semiclassics to get an approximation that we denote as $P() \approx P_{\rm sc}$.

Irrespective of these structural changes, it can be proved that the variance of $P(r)$ is strictly linear and given by the expression

$$\delta E(\delta x) = \sqrt{C(0)}\delta x \equiv \delta E_{\rm cl}. \tag{29}$$

The only assumption that underlines this statement is $\delta x \ll \varepsilon_{\rm cl}$. It reflects the linear departure of the energy surfaces.

5.1. Approximations for $P(n|m)$

The simplest regime is obviously the FOPT regime where, for $P(n|m)$, we can use the standard textbook approximation $P_{\rm FOPT}(n|m) \approx 1$ for $n = m$, while

$$P_{\rm FOPT}(n|m) = \frac{\delta x^2 |\boldsymbol{B}_{nm}|^2}{(E_n - E_m)^2} \tag{30}$$

for $n \neq m$. If outside of the band we have $\boldsymbol{B}_{nm} = 0$, as in the WBRM model, then $P_{\rm FOPT}(r) = 0$ for $|r| > b$. To find the higher order tails (outside of the band) we have to go to higher orders in perturbation theory. Obviously, this approximation makes sense only as long as $\delta x < \varepsilon_c$, where

$$\varepsilon_c = \Delta/\sigma \sim \hbar^{(1+d)/2}, \tag{31}$$

and d is the degrees of freedom of our system ($d = 2$ for the 2D well model). If $\delta x > \varepsilon_c$ but not too large then we still have tail regions which are described by FOPT. This is a non-trivial observation which can be justified by using perturbation theory to infinite order. Then we can argue that a reasonable approximation is

$$P_{\rm prt}(n|m) = \frac{\delta x^2 \ |\boldsymbol{B}_{nm}|^2}{(E_n - E_m)^2 + \Gamma^2}, \tag{32}$$

where Γ is evaluated by imposing normalization of $P_{\rm prt}(n|m)$. In the case of WBRM model $\Gamma = (\sigma\delta x/\Delta)^2 \times \Delta$ [12]. The appearance of Γ in the above expression cannot be obtained from any *finite-order* perturbation theory: formally it requires summation to infinite order. Outside of the bandwidth the tails decay faster than exponentially. Note that $P_{\rm prt}(n|m)$ is a Lorentzian in the case of a flat bandwidth (WBRM model), while in the general case it can be described as a "core-tail" structure.

Obviously, the above approximation makes sense only as long as $\Gamma(\delta x) < \Delta_b$. This expression assumes that the bandwidth Δ_b is sharply defined, as in the WBRM model. By elimination this leads to the determination of $\varepsilon_{\rm prt}$, which in case of the WBRM model is simply

$$\varepsilon_{\rm prt} = \sqrt{b}\varepsilon_c \sim \frac{\hbar}{\tau_{\rm cl}\sqrt{C(0)}}. \tag{33}$$

In more general cases the bandwidth is not sharply defined. Then we have to define the perturbative regime using a practical numerical procedure. The natural definition that we adopt is as follows. We calculate the spreading $\delta E(\delta x)$, which is a linear function. Then we calculate $\delta E_{\rm prt}(\delta x)$, using Eq. (32). This quantity always saturates for large δx because of having finite bandwidth. We compare it to the exact $\delta E(\delta x)$, and define $\varepsilon_{\rm prt}$ for instance as the 80% departure point.

What happens if perturbation theory completely fails? In the WBRM model the LDoS becomes semicircle:

$$P_{\rm sc}(n|m) = \frac{1}{2\pi\Delta}\sqrt{4 - \left(\frac{E_n - E_m}{\Delta}\right)^2}, \tag{34}$$

while in systems that have a semiclassical limit we expect to get

$$P_{\rm sc}(n|m) = \int \frac{{\rm d}Q\,{\rm d}P}{(2\pi\hbar)^d}\,\rho_n(Q,P)\rho_m(Q,P), \tag{35}$$

where $\rho_m(Q,P)$ and $\rho_n(Q,P)$ are the Wigner functions that correspond to the eigenstates $|m(x_0)\rangle$ and $|n(x)\rangle$, respectively.

5.2. The $P(n|m)$ in practice

There are some findings that go beyond the above generic picture and, for completeness, we mention them. The first one is the "localization regime" [35,38,39] which is found in the case of the WBRM model for $\varepsilon > \varepsilon_{\rm loc}$, where

$$\varepsilon_{\rm loc} = b^{3/2}\varepsilon_c. \tag{36}$$

In this regime it is important to distinguish between the non-averaged $P(n|m)$ and the averaged $P(r)$ because the eigenfunctions are non-ergodic but rather localized. This localization is not reflected in the LDoS which is still a semicircle. A typical eigenstate is exponentially localized within an energy range $\delta E_\xi = \xi \Delta$ much smaller than $\delta E_{\rm cl}$. The localization length is $\xi \approx b^2$. In actual physical applications it is not clear whether there is such a type of localization. The above scenario for the WBRM model is summarized in Fig. 7 where we plot $P(n|m)$ in the various regimes. The localized regime is not an issue in the present work and therefore we will no further be concerned with it.

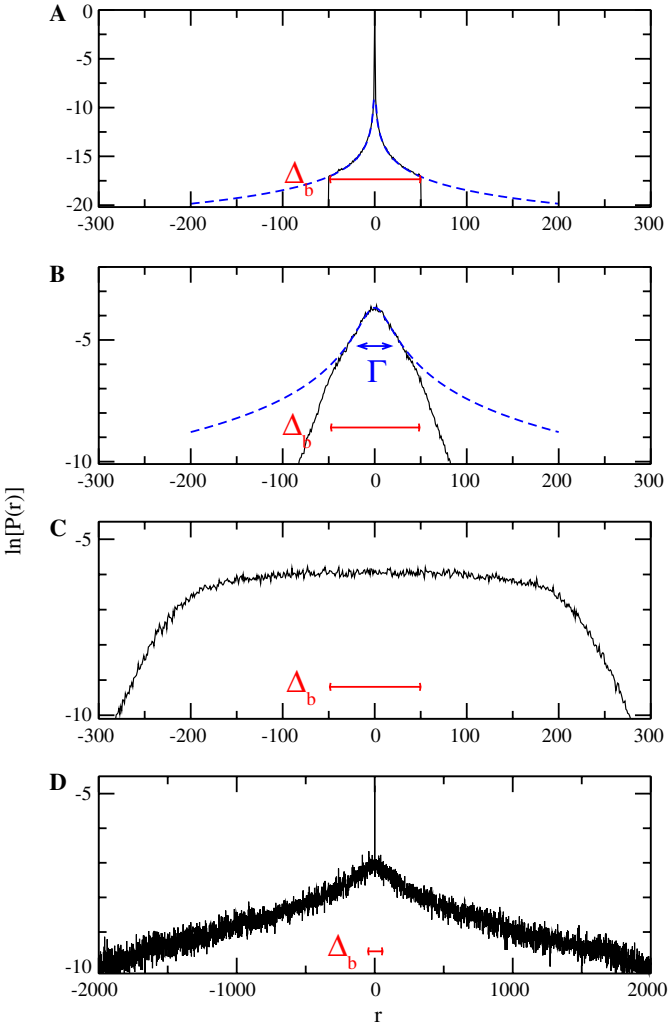

Fig. 7. The parametric evolution of eigenstates of a WBRM model with $\sigma = 1$ and $b = 50$: (A) standard perturbative regime corresponding to $\varepsilon = 0.01$, (B) extended perturbative regime with $\varepsilon = 2$, (C) non-perturbative (ergodic) regime with $\varepsilon = 12$, and (D) localized regime with $\varepsilon = 1$. In (A–C) the mean level spacing $\Delta = 1$ while in (D) $\Delta = 10^{-3}$. The bandwidth $\Delta_b = \Delta \times b$ is indicated in all cases. In (B) the blue dashed line corresponds to a Lorentzian with $\Gamma \approx 16 \ll \Delta_b$ while in (A) we have $\Gamma \approx 10^{-4} \ll \Delta$ which therefore reduces to the standard FOPT result.

The other deviation from the generic scenario, is the appearance of a non-universal "twilight regime" which can be found for some quantized systems [40]. In this regime a co-existence of a perturbative and a semiclassical structure can be observed. For the Pullen–Edmonds model (14) there is no such distinct regime.

For the Hamiltonian model described by Eq. (14) the borders between the regimes can be estimated [19]. Namely $\varepsilon_c \approx 3.8\hbar^{3/2}$ and $\varepsilon_{\rm prt} \approx 5.3\hbar$. In Fig. 8 we report the parametric evolution of the eigenstates for the Hamiltonian model of Eqs. (14) and we compare the outcomes with the results of the EBRM model [19]. Despite the overall quantitative agreement, some differences can be detected:

- In the FOPT regime (see Fig. 8A), the RMT strategy fails in the far tails regime $\Delta \times |r| > \Delta_b$ where system specific interference phenomena become important.
- In the extended perturbative regime (see Fig. 8B) the line-shape of the averaged wavefunction $P(n|m)$ is different from Lorentzian. Still the general features of $P_{\rm prt}$ (core-tail structure) can be detected. In a sense, Wigner's Lorentzian (32) is a special case of core-tail structure. Finally, as in the standard perturbative regime one observes that the far-tails are dominated by either destructive interference (left tail), or by constructive interference (right tail).
- Deep in the non-perturbative regime ($\varepsilon > \varepsilon_{\rm prt}$) the overlaps $P(n|m)$ are well approximated by the semiclassical expression. The exact shape is determined by simple classical considerations [19,42]. This is in contrast to the WBRM model which does not have a classical limit.

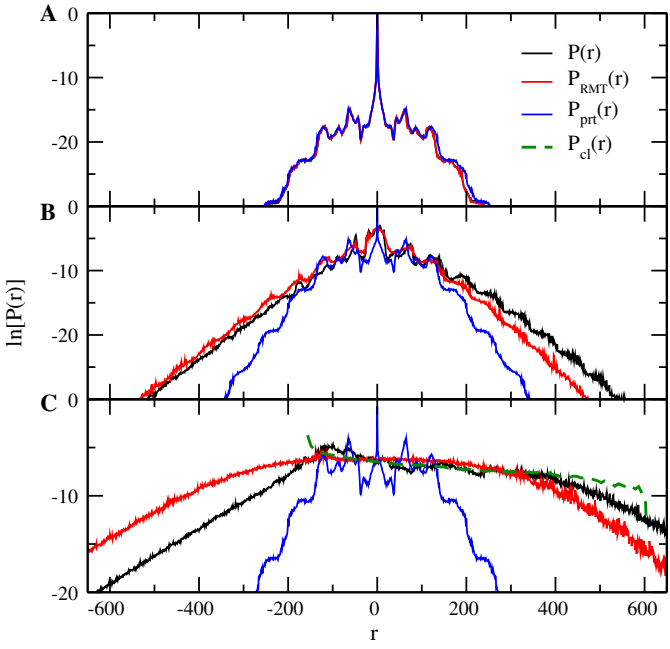

Fig. 8. The quantal profile $P(r)$ for the 2DW model is compared with $P_{\rm prt}(r)$ and with the corresponding $P_{\rm RMT}(r)$ of the EBRM model. The perturbation strength ε is in (A) $\varepsilon = 0.00035$, (B) $\varepsilon = 0.04945$ and (C) $\varepsilon = 0.29$. We are using here the $\hbar = 0.012$ output. In the lower plot the classical LDoS profile $P_{\rm cl}(r)$ is represented by a green heavy dashed line.

6. Linear response theory

The definition of regimes for driven systems is more complicated than the corresponding definition in case of LDoS theory. It is clear that for short times we always can use time-dependent FOPT. The question is, of course, what happens next. There we have to distinguish between two types of scenarios. One type of scenario is *wavepacket dynamics* for which the dynamics is a transient from a preparation state to some new ergodic state. The second type of scenario is *persistent driving*, either linear driving ($\dot{x} = \varepsilon$) or periodic driving ($x(t) = \varepsilon \sin(\Omega t)$). In the latter case, the strength of the perturbation depends on the rate of the driving, not just on the amplitude. The relevant question is *whether the long time dynamics can be deduced from the short time analysis*. To say that the dynamics is of perturbative nature means that the short time dynamics can be deduced from FOPT, while the long time dynamics can be deduced on the basis of a Markovian (stochastic) assumption. The best known example is the derivation of the exponential Wigner law for the decay of a metastable state. The Fermi-Golden-Rule (FGR) is used to determine the initial rate for the escaping process, and then the long-time result is extrapolated by assuming that the decay proceeds in a stochastic-like manner. Similar reasoning is used in deriving the Pauli master equation which is used to describe the stochastic-like transitions between the energy levels in atomic systems.

A related question to the issue of regimes is the validity of linear response theory (LRT). To avoid ambiguities we adopt here a practical definition. Whenever, the result of the calculation depends only on the two point correlation function $C(\tau)$, or equivalently only on the band-profile of the perturbation (which is described by $\tilde{C}(\omega)$), then we refer to it as "LRT." This implies that higher order correlations are not expressed. There is a (wrong) tendency to associate LRT with FOPT. In fact the validity of LRT is not simply related to FOPT. We shall clarify this issue in the next section.

For both $\delta E(t)$ and $\mathcal{P}(t)$ we have "LRT formulas" which we discuss in the next sections. Writing the driving pulse as $\delta x(t) = \varepsilon f(t)$ for the spreading we get

$$\delta E^2(t) = \varepsilon^2 \times \int_{-\infty}^{\infty} \frac{\mathrm{d}\omega}{2\pi} \tilde{C}(\omega) \tilde{F}_t(\omega), \tag{37}$$

while for the survival probability we have

$$\mathcal{P}(t) = \exp\left(-\varepsilon^2 \times \int_{-\infty}^{\infty} \frac{\mathrm{d}\omega}{2\pi} \tilde{C}(\omega) \frac{\tilde{F}_t(\omega)}{(\hbar\omega)^2} \right). \tag{38}$$

Two spectral functions are involved: one is the power spectrum $\tilde{C}(\omega)$ of the fluctuations defined in Eq. (19), and the other $\tilde{F}_t(\omega)$ is the spectral content of the driving pulse which is defined as

$$\tilde{F}_t(\omega) = \left| \int_0^t \mathrm{d}t' \dot{f}(t') \mathrm{e}^{-\mathrm{i}\omega t'} \right|^2. \tag{39}$$

Here, we summarize the main observations regarding the nature of wavepacket dynamics in the various regimes:

- *FOPT regime*. In this regime $\mathcal{P}(t) \sim 1$ for all times, indicating that all probability is all the time concentrated on the initial level. An alternative way to identify this regime is from $\delta E_{\rm core}(t)$ which is trivially equal to Δ.
- *Extended perturbative regime*. The appearance of a core-tail structure which is characterized by separation of scales $\Delta \ll \delta E_{\rm core}(t) \ll \delta E(t) \ll \Delta_b$. The core is of non-perturbative nature, but the variance $\delta E^2(t)$ is still dominated by the tails. The latter are described by perturbation theory.
- *Non-perturbative regime*: The existence of this regime is associated with having the finite energy scale Δ_b. It is characterized by $\Delta_b \ll \delta E_{\rm core}(t) \sim \delta E(t)$. As implied by the terminology, perturbation theory (to any order) is not a valid tool for the analysis of the energy spreading. Note that in this regime, the spreading profile is characterized by a single energy scale ($\delta E \sim \delta E_{\rm core}$).

6.1. The energy spreading $\delta E(t)$

Of special importance for understanding quantum dissipation is the theory for the variance $\delta E^2(t)$ of the energy spreading. Having $\delta E(t) \propto \epsilon$ means *linear response*. If $\delta E(t)/\epsilon$ depends on ϵ, we call it "non-linear response." In this paragraph, we explain that linear response theory (LRT) is based on the "LRT formula" Eq. (37) for the spreading. This formula has a simple classical derivation (see Subsection 6.2 below).

From now on it goes without saying that we assume that the *classical* conditions for the validity of Eq. (37) are satisfied (no $\hbar$ involved in such conditions). The question is *what happens to the validity of LRT once we "quantize" the system*. In previous publications [8,10,11,19], we were able to argue the following:

(A) The LRT formula can be trusted in the perturbative regime, with the exclusion of the adiabatic regime.
(B) In the sudden limit the LRT formula can also be trusted in the non-perturbative regime.
(C) In general the LRT formula cannot be trusted in the non-perturbative regime.
(D) The LRT formula can be trusted deep in the non-perturbative regime, provided the system has a classical limit.

For a system that does not have a classical limit (Wigner model) we were able to demonstrate [8,10,11] that LRT fails in the non-perturbative regime. Namely, for the WBRM model the response $\delta E(t)/\epsilon$ becomes ϵ dependent for large ϵ, meaning that the response is non-linear. Hence, the statement in item (C) above has been established. We had argued that the observed non-linear response is the result of a quantal non-perturbative effect. Do we have a similar type of non-linear response in the case of *quantized chaotic* systems? The statement in item (D) above seems to suggest that the observation of such non-linearity is not likely. Still, it was argued in [11] that this does not exclude the possibility of observing a "weak" non-linearity.

The immediate (naive) tendency is to regard LRT as the outcome of quantum mechanical first order perturbation theory (FOPT). In fact, the regimes of validity of FOPT and of LRT do not coincide. On the one hand, we have the adiabatic regime where FOPT is valid as a leading order description, but not for response calculation. On the other hand, the validity of Eq. (37) goes well beyond FOPT. This leads to the (correct) identification

[7,8,11] of what we call the "perturbative regime." The border of this regime is determined by the energy scale Δ_b, while Δ is not involved. Outside of the perturbative regime we cannot trust the LRT formula. However, as we further explain below, the fact that Eq. (37) is not valid in the non-perturbative regime, does not imply that it *fails* there.

We stress again that one should distinguish between "non-perturbative response" and "non-linear response." These are not synonyms. As we explain in the next paragraph, the adiabatic regime is "perturbative" but "non-linear," while the semiclassical limit is "non-perturbative" but "linear."

In the *adiabatic regime*, FOPT implies zero probability to make a transitions to other levels. Therefore, to the extent that we can trust the adiabatic approximation, all probability remains concentrated on the initial level. Thus, in the adiabatic regime, Eq. (37) is not a valid formula: It is essential to use higher orders of perturbation theory, and possibly non-perturbative corrections (Landau-Zener [1,2]), to calculate the response. Still, FOPT provides a meaningful leading order description of the dynamics (i.e., having no transitions), and therefore we do not regard the adiabatic non-linear regime as "non-perturbative."

In the *non-perturbative regime* the evolution of $P_t(n|m)$ cannot be extracted from perturbation theory: not in leading order, neither in any order. Still it does not necessarily imply a non-linear response. On the contrary: The semiclassical limit is contained in the deep non-perturbative regime [8,11]. There, the LRT formula Eq. (37) is in fact valid. But its validity is *not* a consequence of perturbation theory, but rather the consequence of *quantal-classical correspondence* (QCC).

In the next subsection we will present a classical derivation of the general LRT expression (37). In Subsection 6.3 we derive it using first order perturbation theory (FOPT). In Subsection 6.5, we derive the corresponding FOPT expression for the survival probability.

6.2. Classical LRT derivation for $\delta E(t)$

The classical evolution of $E(t) = \mathcal{H}(Q(t), P(t))$ can be derived from Hamiltonian equations. Namely,

$$\frac{\mathrm{d}E(t)}{\mathrm{d}t} = [\mathcal{H}, \mathcal{H}]_{\mathrm{PB}} + \frac{\partial \mathcal{H}}{\partial t} = -\varepsilon \dot{f}(t)\mathcal{F}(t), \tag{40}$$

where $[\cdot]_{\mathrm{PB}}$ indicates the Poisson Brackets. Integration of Eq. (40) leads to

$$E(t) - E(0) = -\varepsilon \int_0^t \mathcal{F}(t')\dot{f}(t')\,\mathrm{d}t'. \tag{41}$$

Taking a micro-canonical average over initial conditions we obtain the following expression for the variance

$$\delta E^2(t) = \varepsilon^2 \int_0^t C(t'-t'')\dot{f}(t')\dot{f}(t'')\mathrm{d}t'\mathrm{d}t'', \tag{42}$$

which can be re-written in the form of (37).

One extreme special case of Eq. (37) is the sudden limit for which $f(t)$ is a step function. Such evolution is equivalent to the LDoS studies of Section 5. In this case $F_t(\omega) = 1$, and accordingly

$$\delta E_{\mathrm{cl}} = \varepsilon \times \sqrt{C(0)}, \quad \text{[sudden case]}. \tag{43}$$

Another extreme special case is the response for persistent (either linear or periodic) driving of a system with an extremely short correlation time. In such case $F_t(\omega)$ becomes a narrow function with a weight that grows linearly in time. For linear driving ($f(t) = t$) we get $F_t(\omega) = t \times 2\pi\delta(\omega)$. This implies diffusive behavior:

$$\delta E(t) = \sqrt{2D_E t}, \quad \text{[Kubo case]}, \tag{44}$$

where $D_E \propto \epsilon^2$ is the diffusion coefficient. The expression for D_E as an integral over the correlation function is known in the corresponding literature either as Kubo formula, or as Einstein relation, and is the corner stone of the Fluctuation–Dissipation relation.

6.3. Quantum LRT derivation for $\delta E(t)$

The quantum mechanical derivation looks like an exercise in first order perturbation theory. In fact, a proper derivation that extends and clarifies the regime where the result is applicable requires infinite order. If we want to keep a complete analogy with the classical derivation we should work in the adiabatic basis [7]. (For a brief derivation see Appendix D of [9].)

In the following presentation we work in a "fixed basis" and assume $f(t) = f(0) = 0$. We use the standard textbook FOPT expression for the transition probability from an initial state m to any other state n. This is followed by integration by parts. Namely,

$$P_t(n|m) = \frac{\varepsilon^2}{\hbar^2}|\boldsymbol{B}_{nm}|^2\left|\int_0^t \mathrm{d}t' f(t')\mathrm{e}^{\mathrm{i}(E_n - E_m)t'/\hbar}\right|^2 = \frac{\varepsilon^2}{\hbar^2}|\boldsymbol{B}_{nm}|^2\frac{\tilde{F}_t(\omega_{nm})}{(\omega_{nm})^2}, \tag{45}$$

where $\omega_{nm} = (E_n - E_m)/\hbar$. Now we calculate the variance and use Eq. (22) so as to get

$$\delta E^2(t) = \sum\nolimits_n P_t(n|m)(E_n - E_m)^2 = \varepsilon^2\int_{-\infty}^{\infty}\frac{\mathrm{d}\omega}{2\pi}\tilde{C}(\omega)\tilde{F}_t(\omega). \tag{46}$$

6.4. Restricted QCC

The FOPT result for $\delta E(t)$ is *exactly* the same as the classical expression Eq. (37). It is important to realize that there is no $\hbar$-dependence in the above formula. This correspondence does not hold for the higher k-moments of the energy distribution. If we use the above FOPT procedure we get that the latter scale as $\hbar^{k-2}$.

We call the quantum-classical correspondence for the second moment "restricted QCC." It is a very robust correspondence [11]. This should be contrasted with "detailed QCC" that applies only in the semiclassical regime where $P_t(n|m)$ can be approximated by a classical result (and not by a perturbative result).

6.5. Quantum LRT derivation for $\mathcal{P}(T)$

With the validity of FOPT assumed we can also calculate the time-decay of the survival probability $\mathcal{P}(t)$. From Eq. (45) we get

$$p(t) \equiv \sum_{n(\neq n_0)} P_t(n|m) = \varepsilon^2\int_{-\infty}^{\infty}\frac{\mathrm{d}\omega}{2\pi}\tilde{C}(\omega)\frac{\tilde{F}_t(\omega)}{(\hbar\omega)^2}. \tag{47}$$

Assuming that $\mathcal{P}(t) = 1 - p(t)$ can be extrapolated in a "stochastic" fashion we get Eq. (38). Another way to write the final formula is as follows:

$$\mathcal{P}(t) = \exp\left[-\frac{1}{\hbar^2}\int_0^t\int_0^t C(t'-t'')\delta x(t')\delta x(t'')\mathrm{d}t'\mathrm{d}t''\right]. \tag{48}$$

For constant perturbation (wavepacket dynamics) and assuming long times we obtain the Wigner decay,

$$\mathcal{P}(t) = \exp\left[-\left(\frac{\varepsilon}{\hbar}\right)^2\tilde{C}(\omega=0)\times t\right], \tag{49}$$

which can be regarded as a special case of Fermi-Golden-Rule.

6.6. Note on $\mathcal{P}(T)$ for a time reversal scenario

The "LRT formula" for $\mathcal{P}(T)$ in the case of "driving reversal scenario" is

$$\mathcal{P}_{\mathrm{DR}}(t) = \exp\left[-\left(\frac{\varepsilon}{\hbar}\right)^2\int_0^T\int_0^T C(t'-t'')f(t')f(t'')\mathrm{d}t'\mathrm{d}t''\right], \tag{50}$$

where we assumed the simplest scenario with $f(t) = 1$ for $0 < t < (T/2)$ and $f(t) = -1$ for $(T/2) < t < T$. It is interesting to make a comparison with the analogous result in case of "time reversal scenario."

The well known Feynman–Vernon influence functional has the following approximation:

$$\begin{aligned} F[x_A, x_B] &= \langle\Psi|U[x_B]^{-1}U[x_A]|\Psi\rangle \\ &= \exp\left[-\frac{1}{2\hbar^2}\int_0^t\int_0^t C(t'-t'')(x_B(t')-x_A(t'))\quad(x_B(t'')-x_A(t''))\mathrm{d}t'\mathrm{d}t''\right]. \end{aligned} \tag{51}$$

This expression is in fact exact in the case of harmonic bath, and assuming thermal averaging over the initial state. Otherwise, it should be regarded as an extrapolated version of leading order perturbation theory (as obtained in the interaction picture). What people call nowadays "fidelity" or "Loschmidt echo" is in fact a special case of the above expression which is defined by setting $t = T/2$ and $x_A = \varepsilon/2$ while $x_B = -\varepsilon/2$. Thus,

$$\mathcal{P}_{\mathrm{TR}}(t) = |F[x_A, x_B]|^2 = \exp\left[-\left(\frac{\varepsilon}{\hbar}\right)^2\int_0^{T/2}\int_0^{T/2} C(t'-t'')\mathrm{d}t'\mathrm{d}t''\right]. \tag{52}$$

Assuming a very short correlation time one obtains

$$\mathcal{P}_{\mathrm{TR}}(T) = \exp\left[-\frac{1}{2}\left(\frac{\varepsilon}{\hbar}\right)^2\tilde{C}(\omega=0)\times T\right], \tag{53}$$

which again can be regarded as a special variation of the Fermi-Golden-Rule (but note the pre-factor 1/2).

6.7. The survival probability and the LDoS

For constant perturbation it is useful to remember that $\mathcal{P}(t)$ LDoS as follows:

$$\begin{aligned}\mathcal{P}(t) &= \left|\langle n(x_0)|\mathrm{e}^{-\mathrm{i}\mathcal{H}(x)t/\hbar}|n(x_0)\rangle\right|^2 \\ &= \left|\sum_m \mathrm{e}^{-\mathrm{i}E_m(x)t/\hbar}|\langle m(x)|n(x_0)\rangle|^2\right|^2 \\ &= \left|\int_\infty^\infty P(E|m)\mathrm{e}^{-\mathrm{i}Et/\hbar}\mathrm{d}E\right|^2.\end{aligned} \tag{54}$$

This implies that a Wigner decay is associated with a Lorentzian approximation for the LDoS. In the non-perturbative regime the LDoS is not a Lorentzian, and therefore one should not expect an exponential. In the semiclassical regime the LDoS shows system specific features and therefore the decay of $\mathcal{P}(t)$ becomes non-universal.

7. Wavepacket dynamics for constant perturbation

The first evolution scheme that we are investigating here is the so-called *wavepacket dynamics*. The classical picture is quite clear [17,18]: the initial preparation is assumed to be a micro-canonical distribution that is supported by the energy surface $\mathcal{H}_0(Q,P) = E(0)$. Taking $\mathcal{H}$ to be a generator for the classical dynamics, the phase-space distribution spreads away from the initial surface for $t > 0$. 'Points' of the evolving distribution move upon the energy surfaces of $\mathcal{H}(Q,P)$. Thus, the energy $E(t) = \mathcal{H}_0(Q(t),P(t))$ of the evolving distributions spreads with time. Using the LRT formula Eq. (39) for rectangular pulse $f(t') = 1$ for $0 < t' < t$ we get

$$\tilde{F}_t(\omega) = \left|1 - \mathrm{e}^{-\mathrm{i}\omega t}\right|^2 = (\omega t)^2 \mathrm{sinc}^2\left(\frac{\omega t}{2}\right) \tag{55}$$

and hence

$$\delta E_{\mathrm{cl}}(t) = \varepsilon \times \sqrt{2(C(0) - C(t))}. \tag{56}$$

For short times $t \ll \tau_{\mathrm{cl}}$ we can expand the correlation function as $C(t) \approx C(0) - \frac{1}{2}C''(0)t^2$, leading to a ballistic evolution. Then, for $t \gg \tau_{\mathrm{cl}}$, due to ergodicity, a 'steady-state distribution' appears, where the evolving 'points' occupy an 'energy shell' in phase-space. The thickness of this energy shell equals δE_{cl}. Thus, we have a crossover from ballistic energy spreading to saturation:

$$\delta E(t) \approx \begin{cases} \sqrt{2}(\delta E_{\mathrm{cl}}/\tau_{\mathrm{cl}})t & \text{for} \quad t < \tau_{\mathrm{cl}} \\ \sqrt{2}\delta E_{\mathrm{cl}} & \text{for} \quad t > \tau_{\mathrm{cl}} \end{cases}. \tag{57}$$

Fig. 9 shows the classical energy spreading (heavy dashed line) for the 2DW model. In agreement with Eq. (57) we see that $\delta E_{\mathrm{cl}}(t)$ is first ballistic and then saturates. The classical dynamics is fully characterized by the two classical parameters τ_{cl} and δE_{cl}.

7.1. The quantum dynamics

Let us now look at the quantized 2DW model. The quantum mechanical data are reported in Fig. 9 (left panel) where different curves correspond to various perturbation strengths ε. As in the classical case (heavy dashed-line) we observe an initial ballistic-like spreading [18] followed by saturation. This could lead to the wrong impression that the

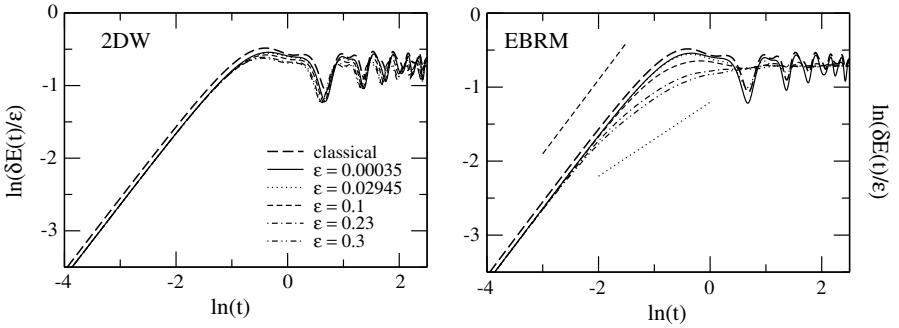

Fig. 9. Simulations of wavepacket dynamics for the 2DW model (left panel) and for the corresponding EBRM model (right panel). The energy spreading $\delta E(t)$ (normalized with respect to the perturbation strength ϵ) is plotted as a function of time for various perturbation strengths ϵ corresponding to different line-types (the same in both panels). The classical spreading $\delta E_{\rm cl}(t)$ (thick dashed line) is plotted in both panels as a reference.

classical and the quantum spreading are of the same nature. However, this is definitely not the case.

To detect the different nature of quantum ballistic-like spreading, one has to inquire measures that are sensitive to the structure of the profile, such as the core-width $\delta E_{\rm core}(t)$. In Fig. 10 we present our numerical data for the 2DW model. If the spreading were of a classical type, it would imply that the spreading profile is characterized by a single energy scale. In such a case we would expect that $\delta E_{\rm core}(t) \sim \delta E(t)$. Indeed this is the case for $\varepsilon > \varepsilon_{\rm prt}$ with the exclusion of very short times: The larger ε is the shorter the quantal transient becomes. In the perturbative regimes, in contrast to the semiclassical regime, we have a separation of energy scales $\delta E_{\rm core}(t) \ll \delta E(t)$. In the perturbative regimes $\delta E(t)$ is determined by the tails, and it is not sensitive to the size of the 'core' region.

Using the LRT formula for $\mathcal{P}(T)$ we get, for short times ($t \ll \tau_{\rm cl}$) during the ballistic-like stage

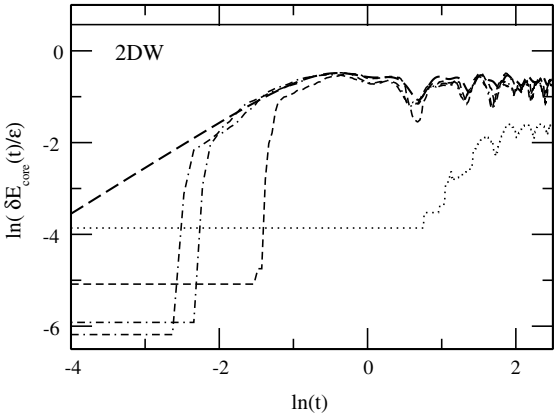

Fig. 10. Simulations of wavepacket dynamics for the 2DW model. The evolution of the (normalized) core width $\delta E_{\rm core}(t)$ is plotted as a function of time. The classical expectation is represented by a thick dashed line for the sake of comparison. As ϵ becomes larger it is approached more and more. We use the same set of parameters as in Fig. 9.

$$\mathcal{P}(t) = \exp\left(-C(\tau = 0) \times \left(\frac{\varepsilon t}{\hbar}\right)^2\right), \tag{58}$$

while for long times ($t \gg \tau_{\rm cl}$) we have the FGR decay of Eq. (49). Can we trust these expressions? Obviously, FOPT can be trusted as long as $\mathcal{P}(t) \sim 1$. This can be converted into an inequality $t < t_{\rm prt}$, where

$$t_{\rm prt} = \left(\frac{\varepsilon_{\rm prt}}{\varepsilon}\right)^{\nu=1,2} \tau_{\rm cl}. \tag{59}$$

The power $\nu = 1$ applies to the non-perturbative regime where the breakdown of $\mathcal{P}(T)$ happens to be before $\tau_{\rm cl}$. The power $\nu = 2$ applies to the perturbative regime where the breakdown of $\mathcal{P}(T)$ happens after $\tau_{\rm cl}$ at $t_{\rm prt} = \hbar/\Gamma$, i.e., after the ballistic-like stage.

The long-term behavior of $\mathcal{P}(T)$ in the non-perturbative regime is not the Wigner decay. It can be obtained by Fourier transform of the LDoS. In the non-perturbative regime the LDoS is characterized by the single energy scale $\delta E_{\rm cl} \propto \delta x$. Hence, the decay in this regime is characterized by a semiclassical time scale $2\pi\hbar/\delta E_{\rm cl}$.

7.2. The EBRM dynamics

Next we investigate the applicability of the RMT approach to describe wavepacket dynamics [17,18] and specifically the energy spreading $\delta E(t)$. At first glance, we might be tempted to speculate that RMT should be able, at least as far as $\delta E(t)$ is concerned, to describe the actual quantum picture. After all, we have seen in Subsection 6.1 that the quantum mechanical LRT formula (46) for the energy spreading involves as its only input the classical power spectrum $\widetilde{C}(\omega)$. Thus we would expect that an effective RMT model with the same band-profile would lead to the *same* $\delta E(t)$.

However, things are not so trivial. In Fig. 9 we show the numerical results for the EBRM model.[2] In the standard and in the extended perturbative regimes we observe a good agreement with Eq. (46). This is not surprising as the theoretical prediction was derived via FOPT, where correlations between off-diagonal elements are not important. In this sense the equivalence of the 2DW model and the EBRM model is trivial in these regimes. But as soon as we enter the non-perturbative regime, the spreading $\delta E(t)$ shows a qualitatively different behavior from the one predicted by LRT: after an initial ballistic spreading, we observe a premature crossover to a diffusive behavior

$$\delta E(t) = \sqrt{2D_{\rm E}t}. \tag{60}$$

The origin of the diffusive behavior can be understood in the following way. Up to time $t_{\rm prt}$ the spreading $\delta E(t)$ is described accurately by the FOPT result (46). At $t \sim t_{\rm prt}$ the evolving distribution becomes as wide as the bandwidth, and we have $\delta E_{\rm core} \sim \delta E \sim \Delta_b$ rather than $\delta E_{\rm core} \ll \delta E \ll \Delta_b$. We recall that in the non-perturbative regime FOPT is subjected to a breakdown before reaching saturation. The following simple heuristic picture turns out to be correct. Namely, once the mechanism for ballistic-like spreading disappears, a stochastic-like behavior takes its place. The stochastic energy spreading is similar to a random-walk process where the step size is of the order Δ_b, with transient time $t_{\rm prt}$. Therefore, we have a diffusive behavior $\delta E(t)^2 = 2D_{\rm E}t$ with

[2] The same qualitative results were found also for the prototype WBRM model, see [17].

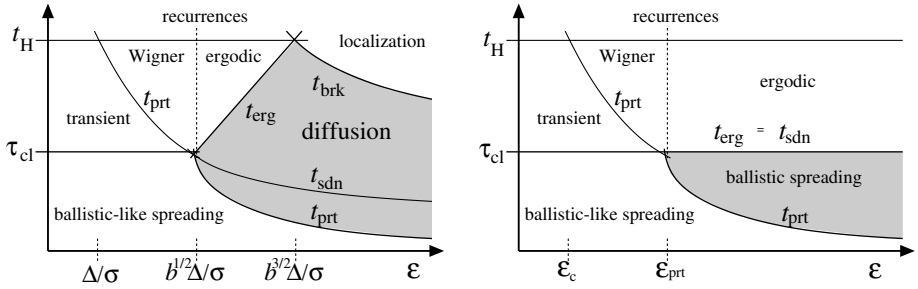

Fig. 11. A diagram that illustrates the various time scales in wavepacket dynamics, depending on the strength of the perturbation ε. The diagram on the left refers to the WBRM model, while that on the right is for a quantized system that has a classical limit. The two cases differ in the non-perturbative regime (large ε): in the case of a quantized model we have a genuine ballistic behavior which reflects detailed QCC, while in the RMT case we have a diffusive stage. In the latter case the times scale t_{sdn} marks the crossover from reversible to non-reversible diffusion. This time scale can be detected in a driving reversal scenario as explained in the next section. For further discussion of this diagram see the text, and in particular the concluding section of this paper.

$$D_E = C \cdot \Delta_b^2/t_{prt} = C \cdot \Delta^2 b^{5/2}\varepsilon\sigma/\hbar \propto \hbar, \tag{61}$$

where C is some numerical pre-factor. This diffusion is not of classical nature, since in the $\hbar \to 0$ limit we get $D_E \to 0$. The diffusion can go on until the energy spreading profile ergodically covers the whole energy shell and saturates to a classical-like steady state distribution. The time t_{erg} for which we get ergodization is characterized by the condition $(D_E t)^{1/2} < \delta E_{cl}$, leading to

$$t_{erg} = b^{-3/2}\hbar\varepsilon\sigma/\Delta^2 \propto 1/\hbar. \tag{62}$$

For completeness we note that for $\varepsilon > \varepsilon_{loc}$ there is no ergodization but rather dynamical ("Anderson" type) localization. Hence, in the latter case, t_{erg} is replaced by the break-time t_{brk}. The various regimes and time scales are illustrated by the diagram presented in Fig. 11.

8. Driving reversal scenario

A thorough understanding of the one-period driving reversal scenario [10] is both important within itself, and for constituting a bridge towards a theory dealing with the response to periodic driving [8]. In the following subsection, we present our results for the prototype WBRM model, while in Subsection 8.2 we consider the 2DW model and compare it to the corresponding EBRM model. The EBRM is better for the purpose of making comparisons with the 2DW, while the WBRM is better for the sake of quantitative analysis (the "physics" of the EBRM and the WBRM models is, of course, the same).

The quantities that monopolize our interest are the energy spreading $\delta E(t)$ and the survival probability $\mathcal{P}(t)$. In Figs. 12 and 13 we present representative plots. From a large collection of such data that collectively span a very wide range of parameters, we extract results for $\delta E(T)$, for $\mathcal{P}(T)$, and for the corresponding compensation times. These are presented in Figs. 12–17.

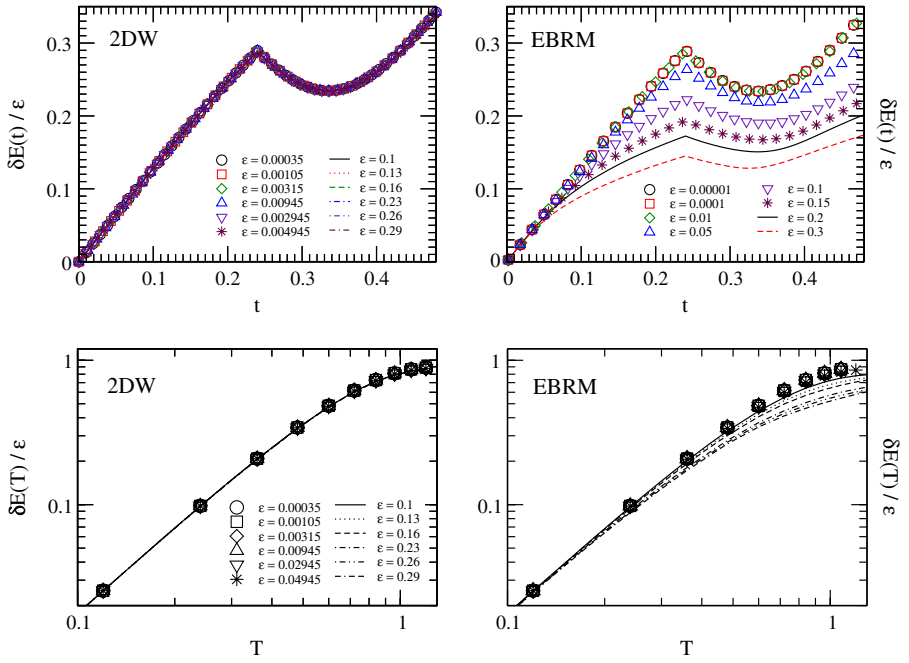

Fig. 12. Simulations of driving reversal for the 2DW model (left panels) and for the corresponding EBRM model (right panels). In the upper row the (normalized) energy spreading $\delta E(t)$ is plotted as a function of time for representative values ε while $T = 0.48$. In the lower row the (normalized) energy spreading $\delta E(T)$ at the end of the cycle is plotted versus T for representative values of ε.

8.1. Driving reversal scenario: RMT case

8.1.1. LRT for the energy spreading

Assuming that the driving reversal happens at $t = T/2$, the spectral content $\tilde{F}_t(\omega)$ for $T/2 < t < T$ is

$$\tilde{F}_t(\omega) = |1 - 2e^{-i\omega T/2} + e^{-i\omega t}|^2. \tag{63}$$

Inserting Eq. (63) into Eq. (37) we get

$$\delta E(t) = \varepsilon \times \sqrt{6C(0) + 2C(t) - 4C\left(\frac{T}{2}\right) - 4C\left(t - \frac{T}{2}\right)}. \tag{64}$$

For the WBRM model we can substitute in Eq. (64) the exact expression Eq. (26) for the correlation function, and get

$$\delta E(t) = 2\varepsilon\sigma \times \sqrt{3b + b\ \mathrm{sinc}\left(\frac{t}{t_{\mathrm{cl}}}\right) - 2b\ \mathrm{sinc}\left(\frac{T}{2\tau_{\mathrm{cl}}}\right) - 2b\ \mathrm{sinc}\left(\frac{t - \frac{T}{2}}{\tau_{\mathrm{cl}}}\right)}. \tag{65}$$

We can also find the compensation time t_r^E by minimizing Eq. (64) with respect to t. For the WBRM model we have

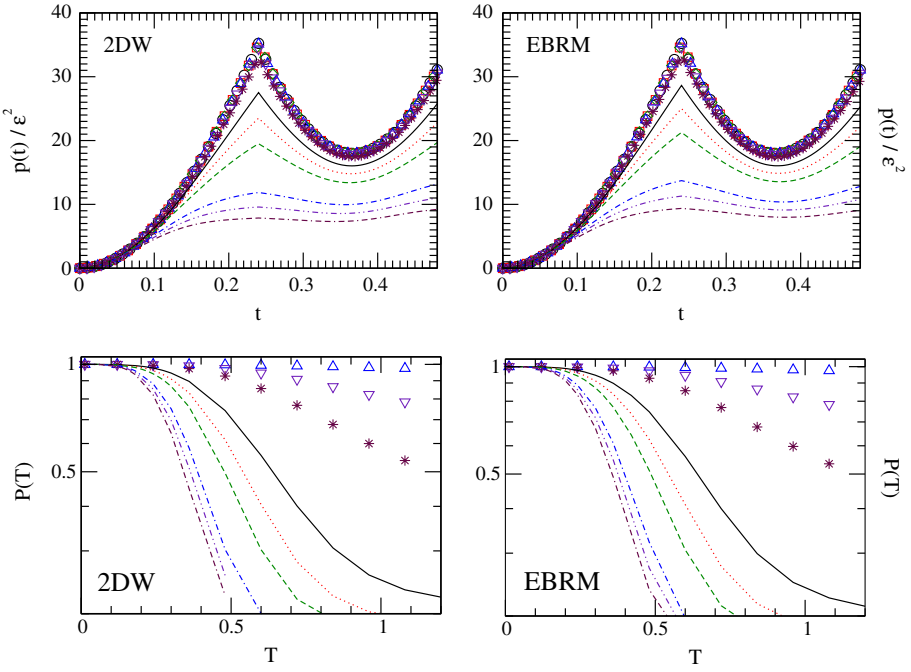

Fig. 13. Simulations of driving reversal for the 2DW model (left panels) and for the corresponding EBRM model (right panels). In the upper row the (normalized) transition probability $p(t) = 1 - \mathcal{P}(t)$ is plotted as a function of time for representative values ε. The period of the driving is $T = 0.48$. In the lower row the survival probability $\mathcal{P}(T)$ at the end of the cycle is plotted versus T for representative values of ε. In all cases we are using the same symbols as in the upper left panel of Fig. 12.

$$\frac{2\cos\left[\frac{T/2-t}{\tau_{\rm cl}}\right]}{\tau_{\rm cl}(T/2-t)} + \frac{2\sin\left[\frac{T/2-t}{\tau_{\rm cl}}\right]}{(T/2-t)^2} + \frac{\cos\left[\frac{t}{\tau_{\rm cl}}\right]}{t\tau_{\rm cl}} = \frac{1}{t^2}\sin\left[\frac{t}{\tau_{\rm cl}}\right], \tag{66}$$

which can be solved numerically to get t_r^E.

The spreading width at the end of the period is

$$\delta E(T) = \varepsilon \times \sqrt{6C(0) + 2C(T) - 8C\left(\frac{T}{2}\right)}. \tag{67}$$

It is important to realize that the dimensional parameters in this LRT analysis are determined by the time scale $\tau_{\rm cl}$ and by the energy scale $\delta E_{\rm cl}$. This means that we have a scaling relation (using units such that $\sigma = \Delta = \hbar = 1$)

$$\frac{\delta E(T)}{\sqrt{b}\varepsilon} = h^E_{\rm LRT}(bT). \tag{68}$$

Deviation from this scaling relation implies a non-perturbative effect that goes beyond LRT.

The LRT scaling is verified nicely by our numerical data (see upper panels of Fig. 14). The values of perturbation strength for which the LRT results are applicable correspond

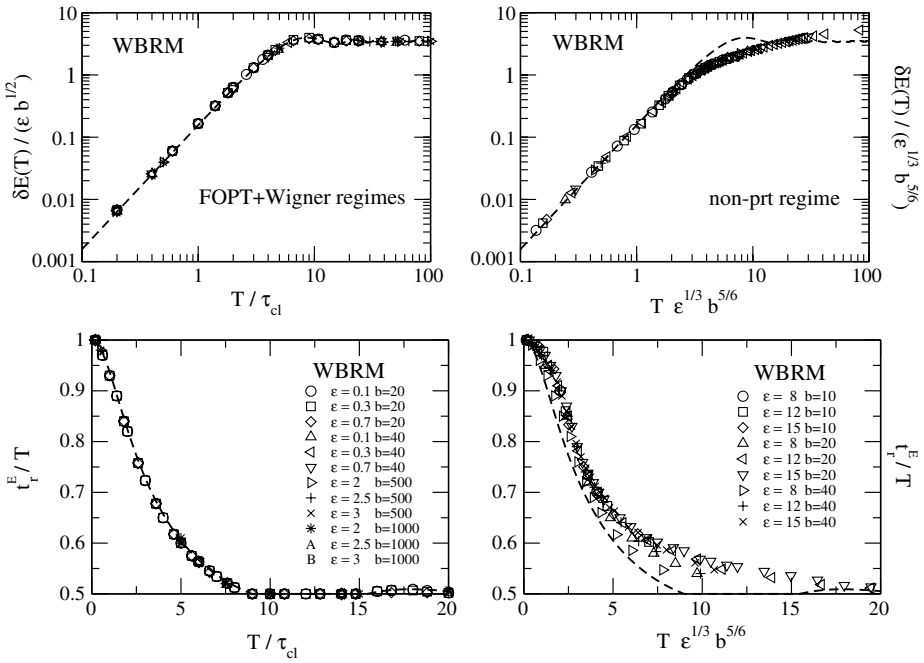

Fig. 14. Simulations of driving reversal for the WBRM model. In the upper row the (scaled) energy spreading $\delta E(T)$ at the end of the cycle is plotted against the (scaled) period T. In the lower panels the compensation time is plotted against the (scaled) period T. The panels on the left are for ε values within the perturbative regime, while the panels on the left are for the non-perturbative regime. For the sake of comparison we plot the LRT expectation for $b = 1$ as a heavy dashed line.

to $\varepsilon < \varepsilon_{\rm prt}$. In the same figure we also plot the whole analytical expression (67) for the spreading $\delta E(T)$. Similarly in Fig. 14 (lower panels) we present our results for the compensation time t_r^E. All the data fall one on top of the other once we rescale them. It is important to realize that the LRT scaling relation implies that the compensation time t_r^E is *independent* of the perturbation strength ε. It is determined only by the *classical* correlation time $\tau_{\rm cl}$. In the same figure, we also present the resulting analytical result (heavy-dashed line) which had been obtained via Eq. (66). An excellent agreement with our data is evident.

8.1.2. Energy spreading in the non-perturbative regime

We turn now to discuss the dynamics in the non-perturbative regime, which is our main interest. In the absence of driving reversal (see Subsection 7.2) we obtain diffusion ($\delta E(t) \propto \sqrt{t}$) for $t > t_{\rm prt}$, where

$$t_{\rm prt} = \hbar/(\sqrt{b}\sigma\varepsilon). \tag{69}$$

If $(T/2) < t_{\rm prt}$, this non-perturbative diffusion does not have a chance to develop, and therefore we can still trust Eq. (64). So the interesting case is $(T/2) > t_{\rm prt}$, which means large enough ε. In the following analysis we distinguish between two stages in the non-perturbative diffusion process. The first stage ($t_{\rm prt} < t < t_{\rm sdn}$) is reversible, while the second stage ($t > t_{\rm sdn}$) is irreversible. For much longer time scales we have recurrences or

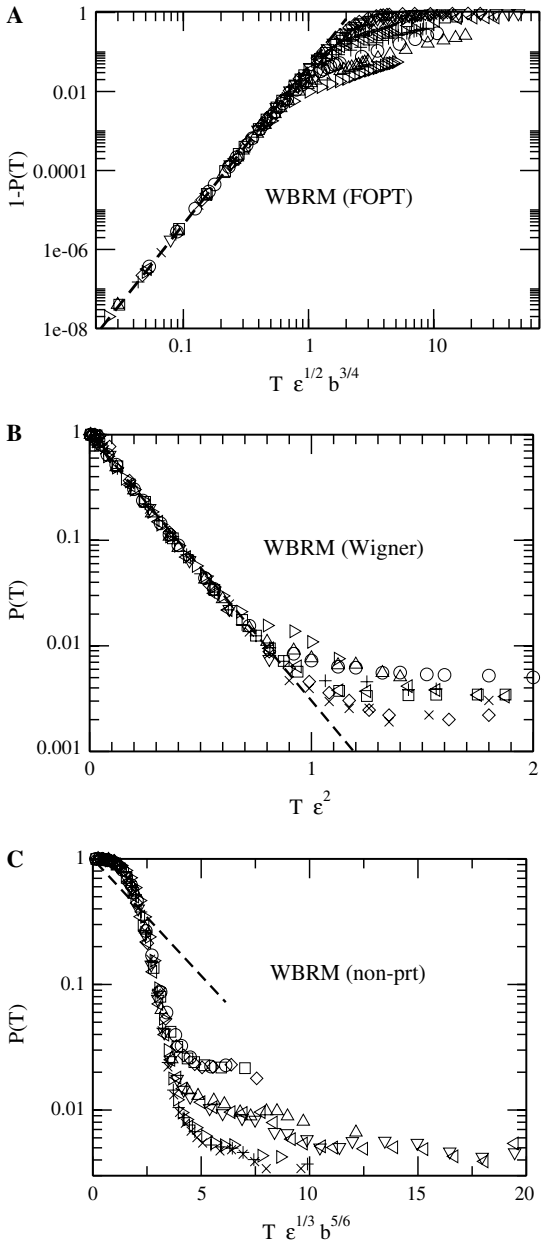

Fig. 15. Simulations of driving reversal for the WBRM model. The survival probability $\mathcal{P}(T)$ at the end of the pulse is plotted against T in the (A) FOPT regime, (B) Wigner regime and (C) non-perturbative regime. In (A) the thick dashed line indicates the super-Gaussian decay (72) while in (B and C) it indicates a Wigner exponential decay (75). Various symbols correspond to different (ε,b) values such that the $\varepsilon < \varepsilon_c$ in (A); $\varepsilon_c < \varepsilon < \varepsilon_{\rm prt}$ in (B) and $\varepsilon > \varepsilon_{\rm prt}$ in (C).

localization, which are not the issue of this paper. The new time scale ($t_{\rm sdn}$) did not appear in our "wavepacket dynamics" study, because it can be detected only in driving reversal experiments.

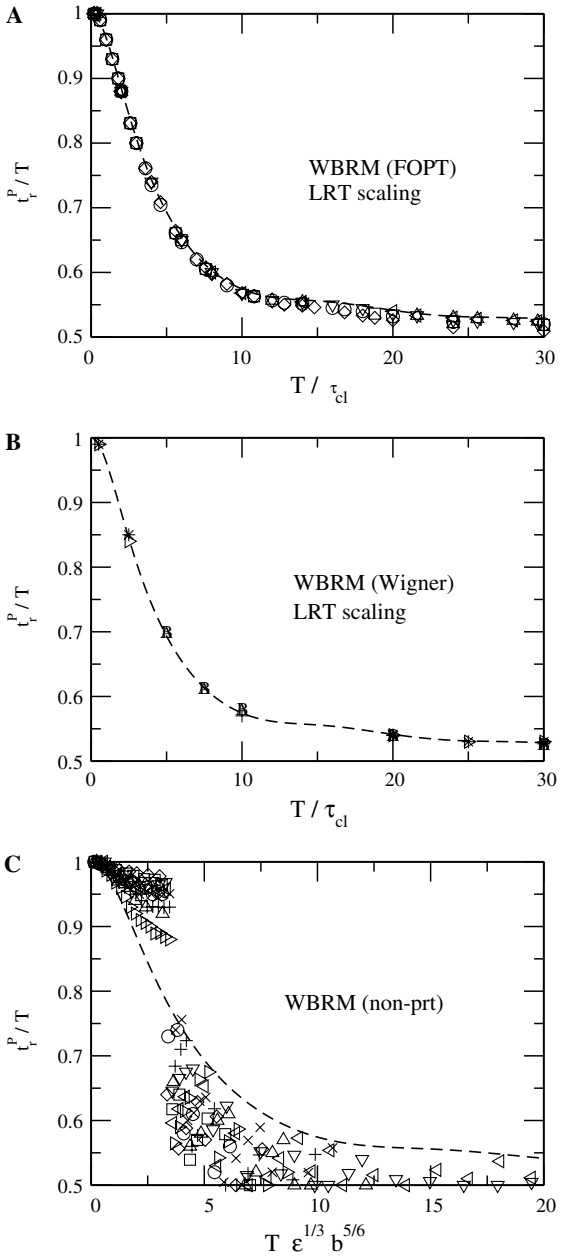

Fig. 16. The compensation time is extracted for the same simulations of the previous figures. Note that for both the FOPT regime and the Wigner regime we have "LRT scaling." The thick dashed line corresponds to the LRT prediction Eq. (74) for $b = 1$. Various symbols correspond to different (ε,b) values such that the $\varepsilon < \varepsilon_c$ in (A); $\varepsilon_c < \varepsilon < \varepsilon_{\text{prt}}$ in (B) and $\varepsilon > \varepsilon_{\text{prt}}$ in (C).

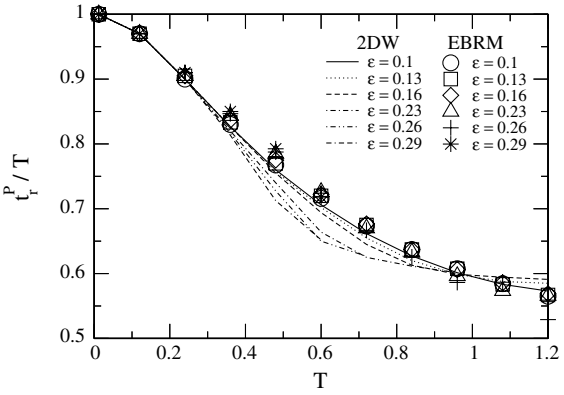

Fig. 17. The compensation time t_r^P for 2DW simulations, and for the corresponding EBRM simulations as a function of T for various values of ε.

The determination of the time scale $t_{\rm sdn}$ is as follows. The diffusion coefficient is $D_{\rm E} = \Delta^2 b^{5/2}\sigma\varepsilon/\hbar$ up to a numerical pre-factor. The diffusion law is $\delta E^2(t) = D_{\rm E} t$. The diffusion process is reversible as long as $\boldsymbol{E}$ does not affect the relative phases of the participating energy levels. This means that the condition for reversibility is $(\delta E(t) \times t)/\hbar \ll 1$. The latter inequality can be written as $t < t_{\rm sdn}$, where

$$t_{\rm sdn} = \left(\frac{\hbar^2}{D_{\rm E}}\right)^{1/3} = \left(\frac{\hbar^3}{\Delta^2 b^{5/2}\sigma\varepsilon}\right)^{1/3}. \tag{70}$$

It is extremely important to realize that without reversing the driving, the presence or the absence of $\mathbf{E}$ in the Hamiltonian cannot be detected. It is only by driving reversal that we can easily determine (as in the upper panels of Fig. 12) whether the diffusion process is reversible or irreversible.

The dimensional parameters in this analysis are naturally the time scale $t_{\rm sdn}$ and the resolved energy scale $\hbar/T$. Therefore, we expect to have instead of the LRT scaling, a different "non-perturbative" scaling relation. Namely, $\delta E(T)/(\hbar/T)$ should be related by a scaling function to $T/t_{\rm sdn}$. Equivalently (using units such that $\sigma = \Delta = \hbar = 1$) it can be written as

$$\frac{\delta E(T)}{b^{5/6}\varepsilon^{1/3}} = h^E_{\rm nprt}(b^{5/6}\varepsilon^{1/3}T). \tag{71}$$

Obviously, the non-perturbative scaling with respect to $\varepsilon^{1/3}$ goes beyond any implications of perturbation theory. It is well verified by our numerical data (see upper right panel of Fig. 14). The values of perturbation strength for which this scaling applies correspond to $\varepsilon > \varepsilon_{\rm prt}$. The existence of the $t_{\rm sdn}$ scaling can also be verified in the lower right panel of Fig. 14, where we show that t_r/T is by a scaling function related to $b^{5/6}\varepsilon^{1/3}T$.

8.1.3. Decay of $\mathcal{P}(T)$ in the FOPT regime

We can substitute Eq. (63) for the spectral content $\tilde{F}_t(\omega)$ of the driving into the LRT formula Eq. (47), and come out with the following expression for the survival probability at the end of the period $t = T$

$$\mathcal{P}(T) \approx \exp(-\varepsilon^2 T^4 b^3). \tag{72}$$

This is a super-Gaussian decay, which is quite different from the standard Gaussian decay Eq. (58) or any other results on reversibility that appear in literature [20–24]. We have verified that this expression is valid in the FOPT regime. See Fig. 15A.

For the WBRM model, we get the following expression for $p(t)$ after substituting the spectral content $\tilde{F}_t(\omega)$ given from Eq. (63)

$$p(t) = \frac{(\varepsilon\sigma)^2}{\Delta\hbar} \times \int_{-\omega_{\rm cl}}^{\omega_{\rm cl}} \mathrm{d}\omega \frac{6 - 4[\cos(\frac{\omega T}{2}) + \cos(\omega(t - \frac{T}{2}))] + 2\cos(\omega t)}{\omega^2}. \tag{73}$$

The corresponding compensation time t_r^P can be found after minimizing the above expression (corresponding to the maximization of $\mathcal{P}(t) = 1 - p(t)$) with respect to time t. This results in the following equation:

$$\mathrm{si}(\omega_{\rm cl} t) = 2\mathrm{si}\left(\omega_{\rm cl}\left(t - \frac{T}{2}\right)\right), \tag{74}$$

which has to be solved numerically to evaluate t_r^P. Above $\mathrm{si}(x) = \int_0^x \frac{\sin x}{x}$. Our numerical data are reported in Fig. 16 together with the theoretical prediction (74).

8.1.4. Decay of $\mathcal{P}(T)$ in the Wigner regime

We now turn to discuss $\mathcal{P}(t)$ in the "Wigner regime." By this we mean $\varepsilon_c < \varepsilon < \varepsilon_{\rm prt}$. This distinction does not appear in the $\delta E(t)$ analysis. The time evolution of $\delta E(t)$ is dominated by the tails of the distribution and does not affect the "core" region. Therefore, $\delta E(t)$ also agreed with LRT outside of the FOPT regime in the whole (extended) perturbative regime. But this is not the case with $\mathcal{P}(t)$, which is mainly influenced by the "core" dynamics. As a result in the "Wigner regime" we get different behavior compared with the FOPT regime.

We look at the survival probability $\mathcal{P}(T)$ at the end of the driving period. In the Wigner regime, instead of the LRT-implied super-Gaussian decay, we find a Wigner-like decay:

$$\mathcal{P}(T) \approx \mathrm{e}^{-\Gamma(\varepsilon)T}, \tag{75}$$

where $\Gamma \approx \varepsilon^2/\Delta$. In Fig. 15B we present our numerical results for various perturbation strengths in this regime. A nice overlap is observed once we rescale the time axis as $\varepsilon^2 \times T$. We would like to emphasize once more that both in the standard and in the extended perturbative regimes the scaling law involves the perturbation strength ε. This should be contrasted with the LRT scaling of $\delta E(t)$.

What about the compensation time t_r^P? A reasonable assumption is that it will exhibit a different scaling in the FOPT regime and in the Wigner regime (as is the case of $\mathcal{P}(T)$). Namely, in the FOPT regime we would expect "LRT scaling" with $\tau_{\rm cl}$, while in the Wigner regime we would expect "Wigner scaling" with $t_{\rm prt} = \hbar/\Gamma$. The latter is of non-perturbative nature and reflects the "core" dynamics. To our surprise we find that this is not the case. Our numerical data presented in Fig. 16 show beyond any doubt that the "LRT scaling" applies within the whole (extended) perturbative regime, as in the case of t_r^E, thus not invoking the perturbation strength ε. We see that the FOPT expression (74) for t_r^P shown as a heavy-dashed line describes the numerical findings.

We conclude that the compensation time t_r is mainly related to the dynamics of the tails, and hence can be deduced from the LRT analysis.

8.1.5. Decay of $\mathcal{P}(T)$ in the non-perturbative regime

Let us now turn to the non-perturbative regime (see Fig. 15C). As in the case of the spreading kernel $\delta E(T)$, the decay of $\mathcal{P}(T)$ is no longer captured by perturbation theory. Instead, we observe the same non-universal scaling with respect to $\varepsilon^{1/3} \times T$ as in the case of $\delta E(T)$.

$$\mathcal{P}(T) = h^{P}_{\mathrm{nprt}}(b^{5/6}\varepsilon^{1/3}T). \tag{76}$$

The reason is that in the non-perturbative regime the two energy scales Γ and Δ_b, which were responsible for the difference between $\mathcal{P}(T)$ and $\delta E(T)$, lose their meaning. As a consequence, the spreading process involves only one time scale and the behavior of both $\mathcal{P}(T)$ and $\delta E(T)$ becomes similar, leading to the same scaling behavior.

8.2. Driving reversal scenario: 2DW case

In the representative simulations of the 2DW model in Fig. 12 (upper left panel) we see that the spreading $\delta E(t)$ for $T = 0.48$ and various perturbation strengths ε follows the LRT predictions very well. Fig. 12 (lower left panel) shows that the agreement with the LRT is observed for any value of the period T. This stands in clear contrast to the EBRM model shown in Fig. 12 (right panels).

The agreement with LRT in the non-perturbative regime, as in the case of wavepacket dynamics, reflects detailed QCC. We recall that "to get into the non-perturbative regime" and "to make $\hbar$ small" means the same. All our simulations are done in a regime where LRT can be trusted at the classical (= non-perturbative) limit. It is only for RMT models that we observe a breakdown of LRT trusted in the non-perturbative regime.

What about $\mathcal{P}(T)$? This quantity has no classical analogue. Therefore, QCC considerations are not applicable. Also LDoS considerations cannot help here. The one-to-one correspondence between the LDoS and the survival probability applies to the simple wavepacket dynamics scenario (constant perturbation).

It is practically impossible to make a quantitative analysis of $\mathcal{P}(T)$ in the case of a real model because the band-profile is very structured and there are severe numerical limitations. Rather, what we can easily do is to compare the 2DW with the corresponding EBRM. Any difference between the two constitutes an indication for a non-perturbative effect. Representative simulations are presented in Fig. 13.

In Fig. 17 we show the dependence of the compensation time t_r^P on T for the EBRM model. We see very nice scaling behavior that indicates that our numerics (as far as $\mathcal{P}(T)$ is concerned!) is limited to the perturbative regime. We emphasize again that the physics of $\mathcal{P}(T)$ is very different from the physics of $\delta E(T)$. Therefore, this finding by itself should not be regarded as very surprising. A sharp crossover to a non-perturbative behavior can be expected for a "sharp" band-profile only (which is the WBRM and not the EBRM—see Fig. 16).

Now we switch from the EBRM model to the 2DW model. Do we see any deviation from LRT scaling? The answer from Fig. 17 is clearly yes, as reflected by the ε dependence of the curve. The effect is small, but "it is there." It indicates that the "body" of the probability distribution, in the case of the 2DW dynamics, does not evolve the same way as in the EBRM case. Indeed we know that the main part of the distribution evolves faster (in a ballistic fashion rather than diffusively), and therefore we observe lower values of t_r^P.

Assuming that the decay of $\mathcal{P}(T)$ is given by the exponential law, we extract the corresponding decay rates γ. It should be clear that the fitting is done merely to extract

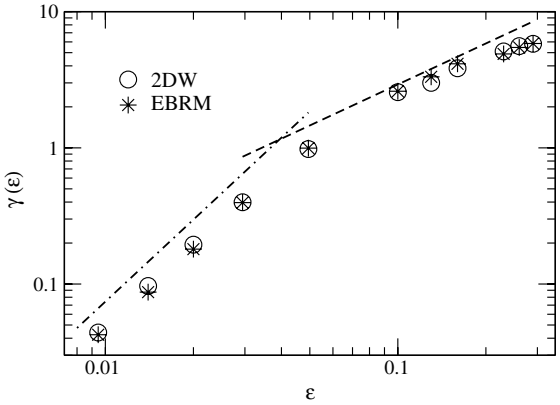

Fig. 18. The estimated decay rate γ for the same simulations as in the previous figure.

a numeric measure for the behavior of the decay. We would not like to suggest that the decay looks strictly exponential. The results are reported in Fig. 18. We find that for $\varepsilon < \varepsilon_{\rm prt}$, the decay rate $\gamma(\varepsilon) \propto \varepsilon^2$, as expected by Wigner's theory, while for $\varepsilon > \varepsilon_{\rm prt}$ we find that $\gamma \propto \varepsilon$. This linear dependence on ε is essentially the same as in the corresponding wavepacket dynamics scenario. There it is clearly associated with the width $\delta E_{\rm cl} \propto \varepsilon$ of the LDoS.

As far as γ is concerned the behavior of 2DW and the EBRM models are the same, and there is an indication of the crossover from the perturbative to the non-perturbative regime, as implied (in a non-rigorous fashion) by the LDoS theory. It is t_r^P rather than γ that exhibits sensitivity to the nature of the dynamics. This is because t_r^P is sensitive to the evolution of the main part of the distribution. We already had made this observation on the basis of the analysis of the WBRM model (see previous Subsection 8.1). Here, we see another consequence of this observation.

9. Conclusions

There is a hierarchy of challenges in the study of quantum dynamics. The simple way to explain this hierarchy is as follows: let us assume that there are two Hamiltonians, $\mathcal{H}_1$ and $\mathcal{H}_2$, that differ slightly from each other. Let us then quantify the difference by a parameter ε. Let us distinguish between a FOPT regime, Wigner regime, and non-perturbative (semi-circle or semiclassical) regime according to the line shape of the LDoS. *Do we have enough information to say something about the dynamics?*

In the conventional wavepacket dynamics, one Hamiltonian is used for preparation and for measurement, while the other for propagation. It is well known that the Fourier transform of the LDoS gives the survival amplitude and hence $\mathcal{P}(t)$. But what about other features of the dynamics. What about the energy spreading $\delta E(t)$ for example? It turns out that the answer requires more than just knowing the LDoS. In particular we observe that in the non-perturbative regime physical models differ from the corresponding RMT model. In the former case we have ballistic spreading while in the latter we have diffusion.

Is there any new ingredient in the study of driving reversal dynamics? *Maybe it is just a variation on conventional wavepacket dynamics?* The answer turns out to be interesting.

There is a new ingredient in the analysis. This becomes very clear in the RMT analysis where we find a new time scale that distinguishes between a stage of "reversible diffusion" and a stage of "irreversible diffusion." This time scale ($t_{\rm sdn}$) can only be probed in a driving reversal experiment. It is absent in the study of conventional wavepacket dynamics.

Things become more interesting, and even surprising, once we get into details. Let us summarize our main findings. We start with the conventional wavepacket dynamics, and then turn to the driving reversal scenario.

The main observations regarding wavepacket dynamics are summarized by the diagrams in Fig. 11. We always have an initial ballistic-like stage which is implied by FOPT. During this stage the first order (in-band) tails of the energy distribution grow like t^2. We call this behavior "ballistic-like" because the second moment $\delta E(t)$ grows like t^2. It is not a genuine ballistic behavior because the rth moment does not grow like t^r but rather all the moments of this FOPT distribution grow like t^2.

The bandwidth Δ_b is resolved at the time $\tau_{\rm cl}$. In the perturbative regime this happens before the breakdown of perturbation theory, while in the non-perturbative regime the breakdown $t_{\rm prt}$ happens before $\tau_{\rm cl}$. As a result, in the non-perturbative regime we can get a non-trivial spreading behavior which turns out to be "ballistic" or "diffusive," depending on whether the system has a classical limit or is being RMT modeled.

Once we consider a driving reversal scenario, it turns out to be important to mark the time $t_{\rm sdn}$ when the energy distribution is resolved. The question is ill-defined in the perturbative regime because there the energy distribution is characterized by two energy scales (the "bandwidth" and the much smaller "core width"). But the question is well-defined in the non-perturbative regime where the distribution is characterized by one energy scale. It is not difficult to realize that for ballistic behavior $t_{\rm sdn} \sim \tau_{\rm cl}$ which is also the classical ergodic time. But for diffusion we get a separation of time scales $t_{\rm prt} \ll t_{\rm sdn} \ll \tau_{\rm cl}$. Thus, we conclude that the diffusion has two stages: One is reversible while the other is irreversible.

But the second moment does not fully characterize the dynamics. In the other extreme we have the survival probability. Whereas $\delta E(T)$ is dominated by the tails, $\mathcal{P}(T)$ is dominated by the "core" of the distribution. Therefore, it becomes essential to distinguish between the FOPT regime where the "core" is just one level, and the rest of the perturbative regime (the "Wigner" regime) where the core is large (but still smaller compared with the bandwidth).

The main findings regarding the driving reversal scenario are summarized by the following table:

Regime	Perturbation strength	$\mathcal{P}(T)$ behavior	t_r behavior	$\delta E(T)$ behavior
First order perturbative	$\varepsilon < \varepsilon_c$	LRT (super-Gaussian)	LRT	LRT (ballistic-like)
Extended perturbative ("Wigner")	$\varepsilon_c < \varepsilon < \varepsilon_{\rm prt}$	Wigner (Exponential)	LRT(!)	LRT (ballistic-like)
Non-perturbative	$\varepsilon > \varepsilon_{\rm prt}$	Non-perturbative (non-universal)	Non-perturbative (non-universal)	Non-perturbative[a] (diffusive/ballistic)

[a] For the WBRM we have diffusion while for the 2DW model we have ballistic behavior as implied by classical LRT.

As expected we find that $\mathcal{P}(T)$ obeys FOPT behavior in the FOPT regime, which turns out to be super-Gaussian decay. In the Wigner regime $\delta E(T)$ still obeys LRT because the tails obey FOPT, while the non-perturbative core barely affects the second moment. But in contrast to that $\mathcal{P}(T)$ is sensitive to the core, and therefore we find Wigner (exponential) decay rather than FOPT (super-Gaussian) behavior. However, when we look more carefully at the whole $\mathcal{P}(T)$ curve, we find that this is not the whole story. We can characterize $\mathcal{P}(T)$ by the compensation time t_r. It turns out that t_r is sensitive to the nature of the dynamics. Consequently it obeys "LRT scaling" rather than "Wigner scaling." This has further consequences that are related to quantal-classical correspondence. Just by looking at $\mathcal{P}(T)$ we cannot tell whether we look at the "real simulation" or on its RMT modeling. But looking on t_r we can find a difference. It turns out that in the physical model t_r exhibits ε dependence, while in the case of RMT modeling t_r is independent of ε and exhibits "LRT-scaling."

Finally, we come to the non-perturbative regime. Here we have, in a sense a simpler situation. We have only one energy scale, and hence only one time scale, and therefore $\delta E(T)$ and $\mathcal{P}(T)$ essentially obey the same scaling. Indeed we have verified that the non-perturbative scaling with $t_{\rm sdn}$ in WBRM simulations is valid for both the second moment and the survival probability.

Finally, we would like to emphasize that the notion of "non-perturbative" behavior should not be confused with "non-linear" response. In case of quantized models, linear response of the energy spreading $\delta E(T)$ is in fact a consequence of non-perturbative behavior. This should be contrasted with the WBRM model, where QCC does not apply, and indeed deviations from the linear response appear once we enter the non-perturbative regime.

The study of irreversibility in a simple driving reversal scenario is an important step towards the understanding of irreversibility and dissipation in general. The analysis of dissipation reduces to the study of energy spreading for time-dependent Hamiltonians $\mathcal{H}(Q,P;x(t))$. In generic circumstances the rate of energy absorption is determined by a diffusion-dissipation relation: The long time process of dissipation is determined by the short time diffusion process. The latter is related to the fluctuations $\tilde{C}(\omega)$ via what we call "LRT formula". Thus the understanding of short time dynamics is the crucial step in establishing the validity of the fluctuation-dissipation relation.

Acknowledgments

This research was supported by a grant from the GIF, the German-Israeli Foundation for Scientific Research and Development, and by the Israel Science Foundation (Grant No.11/02).

References

[1] M. Wilkinson, J. Phys. A 20 (1987) 2415.
[2] M. Wilkinson, J. Phys. A 21 (1988) 4021.
[3] M. Wilkinson, E. Austin, J. Phys. A 28 (1995) 2277.
[4] A. Bulgac, G.D. Dang, D. Kusnezov, Phys. Rev. E 54 (1996) 3468.
[5] U. Weiss, Quantum Dissipative Systems, World Scientific, 1998.
[6] M. Wilkinson, Parametric Random Matrices: Static and Dynamic Applications, Kluwer Academic/Plenum Publishers, New York, 1999, pp. 369–399.

[7] D. Cohen, Ann. Phys. 283 (2000) 175.
[8] D. Cohen, T. Kottos, Phys. Rev. Lett. 85 (2000) 4839.
[9] D. Wisniacki, D. Cohen, Phys. Rev. E 66 (2002) 046209.
[10] T. Kottos, D. Cohen, Europhys. Lett. 61 (2003) 431.
[11] D. Cohen, T. Kottos, J. Phys. A 36 (2003) 10151.
[12] E. Wigner, Ann. Math. 62 (1955) 548.
[13] E. Wigner, Ann. Math. 65 (1957) 203.
[14] H.-J. Stöckmann, Quantum Chaos: An Introduction, University Press, Cambridge, 1998.
[15] F. Haake, Quantum Signatures of Chaos, Second edition., Springer-Verlag, Berlin, Heidelberg, New York, 2000.
[16] Y. Alhassid, Rev. Mod. Phys. 72 (2000) 895.
[17] D. Cohen, F. Izrailev, T. Kottos, Phys. Rev. Lett. 84 (2000) 2052.
[18] T. Kottos, D. Cohen, Phys. Rev. E 64 (2001) 0652021.
[19] D. Cohen, T. Kottos, Phys. Rev. E 63 (2001) 036203.
[20] T. Prosen, T.H. Seligman, J. Phys. A 35 (2002) 4707.
[21] G. Benenti, G. Casati, Phys. Rev. E 66 (2002) 066205.
[22] R. Jalabert, H. Pastawski, Phys. Rev. Lett. 86 (2001) 2490.
[23] C.B.Ph. Jacquod, I. Adagideli, Phys. Rev. Lett. 89 (2002) 154103.
[24] M. Hiller, T. Kottos, D. Cohen, T. Geisel, Phys. Rev. Lett. 92 (2004) 010402.
[25] R.A. Pullen, A.R. Edmonds, J. Phys. A 14 (1981) L477.
[26] H.D. Meyer, J. Chem. Phys. 84 (1986) 3147.
[27] O. Bohigas, M. Giannoni, C. Schmidt, Phys. Rev. Lett. 52 (1984) 1.
[28] M. Feingol, A. Peres, Phys. Rev. A 34 (1986) 591.
[29] M. Berry, Chaos and Quantum Systems, Elsevier, 1991.
[30] Y. Imry, Introduction to Mesoscopic Physics, Oxford University Press, New York, Oxford, 1997.
[31] M. Berry, J. Phys. A 10 (1977) 2083.
[32] T. Prosen, M. Robnik, J. Phys. A 26 (1993) L319.
[33] T. Prosen, Ann. Phys. 235 (1994) 115.
[34] E. Austin, M. Wilkinson, Nonlinearity 5 (1992) 1137.
[35] M. Feingold, D. Leitner, M. Wilkinson, Phys. Rev. Lett. 66 (1991) 986.
[36] M. Feingold, A. Gioletta, F. Izrailev, L. Molinari, Phys. Rev. Lett. 70 (1993) 2936.
[37] Y. Fyodorov, O. Chubykalo, F. Izrailev, G. Casati, Phys. Rev. Lett. 76 (1996) 1603.
[38] G. Casati, L. Molinari, F. Izrailev, Phys. Rev. Lett. 64 (1990) 1851.
[39] G. Casati, I. Guarneri, R. Scharf, F. Izrailev, Phys. Rev. Lett. 64 (1990) 5.
[40] J.A. Méndez-Bermúdez, T. Kottos, D. Cohen, Phys. Rev. E 72 (2005) 027201.
[41] F. Izrailev, T. Kottos, A. Politi, G. Tsironis, Phys. Rev. E 55 (1997) 4951.
[42] F. Borgonovi, I. Guarneri, F. Izrailev, Phys. Rev. E 57 (1998) 5291.